



This is an author produced version of *Behaviour of Restrained Steel Beam with Reduced Beam Section Exposed to Fire*.

White Rose Research Online URL for this paper:  
<http://eprints.whiterose.ac.uk/98683/>

---

**Article:**

Guo, Z. and Huang, S. [orcid.org/0000-0003-2816-7104](https://orcid.org/0000-0003-2816-7104) (2016) Behaviour of Restrained Steel Beam with Reduced Beam Section Exposed to Fire. *Journal of Constructional Steel Research*, 122. pp. 434-444. ISSN 0143-974X

<https://doi.org/10.1016/j.jcsr.2016.04.013>

---

## Behaviour of Restrained Steel Beam with Reduced Beam Section Exposed to Fire

Zhen Guo<sup>a\*</sup>, Shan-Shan Huang<sup>b</sup>

<sup>a</sup> *School of Mechanics & Civil Engineering, China University of Mining and Technology, Xu zhou 221116, China*

<sup>b</sup> *Department of Civil & Structural Engineering, The University of Sheffield, Sir Frederick Mappin Building, Mappin Street, Sheffield S1 3JD, UK*

### Abstract

Reduced beam section (RBS) is one of the connection types, which is economical and popular for use in steel moment frames in seismic regions. By cutting some portions of the beam flanges near the column face, the RBS connections are designed to form plastic hinge within the RBS zone so that it could enhance the structural seismic performance. However, the steel beams with RBS connections have to provide robustness when exposed to fire. Although the responses of ordinary steel beams to elevated temperatures have been investigated over the last few decades, there has been very limited research on the behaviour of steel beams, with RBS connections in fire. This study includes a series of numerical analysis, to investigate the high-temperature performance of steel beams with RBS connections, compared to the responses of ordinary steel beams to fire. Various parameters have been considered, including the types of fire curves, the levels of beam-end restraints and the cutting profiles of the RBS connections. Overall, the deformation shape of RBS beams at high temperature is similar to that of ordinary steel beams, whereas the RBS beams could have longer period of fire resistance. The cut section actually provides both rotational and axial ductility/deformability to the connection, enhancing its fire resistance. Moreover, the cutting length, proposed by EC8, is also adequate for fire design. The minimum distance, between the RBS zone and the beam-end, proposed by FEMA-350 has been shown sufficient.

Keywords: Reduced Beam Section (RBS); Steel Connections; Fire; Moment Frame.

---

\* Corresponding author: Tel.:+86 516 83590666; fax: +86 516 83884360

E-mail addresses: z.guo@cumt.edu.cn (Zhen Guo)

## 1. Introduction

After the 1994 Northridge[1] and 1995 Kobe earthquakes [2], the reduced beam section (RBS) joints have been extensively used in steel moment resisting frames (MRFs) to avoid brittle fractures of beam-to-column connections as observed in these two hazards [3]. The RBS joints, with portion of beam flanges near beam-to-column connections being cut[4], are designed to form a plastic hinge away from a connection so that beams (rather than the beam-to-column interface) could develop ductility, as shown in Fig.1. In this figure,  $M_{sd}$  is the design bending moment;  $M_{pl}$  is the cross-sectional bending resistance; and  $M_{pl-RBS}$  is the sectional plastic moment resistance at RBS zone. As indicated by several quasi-static tests [5] [6], RBS has excellent energy dissipation capacities under cyclic loads, in terms of forming plastic hinge in the RBS zone and protecting the connection and the connected elements.

The design requirements of connection for fire[7] and that for earthquake [8-10] are very different. In seismic design, it is required that a plastic hinge is formed at the RBS zone to provide sufficient rotational ductility. However, for fire design, connections need to be able to resist very high forces along the axis of the beam; either large compression due to restrained thermal expansion during initial heating or large tension due to the very large beam deflection in the catenary tension phase [11]. The RBS beams, with the flanges cut to provide ductility required by seismic design, may have lower flexural and tensile capacities and poorer fire performance than those of ordinary beams. However, there has been very limited research on the fire resistance of RBS beams, which is worth investigating.

The RBS zone is vulnerable to tensile fracture at high temperature, as indicated in existing fire tests [12-14] on isolated RBS joints. Moreover, the location of the cut section and the depth of circular cutting will affect the behaviour of a beam in fire. Using numerical analysis, Lee *et al.* [15] found that, unlike ordinary beam-to-column connections, RBS joints subject to fire, mainly failed by local buckling at the top flange and web of the RBS region. However, the effects of the geometrical size of

the RBS zone and the beam-end restraints on the fire resistance of RBS joint have not been investigated. The beam-end restraints (both rotational and axial) will affect the internal force distribution and hence affect the behaviour of connection, whereas this effect needs to be quantified.

This paper presents an investigation on RBS beams, considering the effects of geometrical size of RBS, beam-end restraint and fire temperature-time relationship, on the high-temperature performance of RBS beam at elevated temperatures. The robustness of RBS connections in fire is the main concern of this research, and so more attention has been put on to the fracture time/temperature rather than on the ultimate load/moment capacities. The effects of the supported concrete slab on the temperature distribution in the connection and beam, have also been taken into account.

## **2. High-temperature performance of ordinary steel beam in fire**

The high-temperature performance of ordinary steel beams has been studied widely in the world over the last few decades [16][17]. This section summarizes typical behaviour of ordinary (non-RBS) steel beams in fire.

### ***2.1 Structural damage of steel beams in fire tests***

The local buckling in the beam web or flange is a common failure mode, when steel beams are exposed to fire without any fire protection. Fig.2(a) shows the local buckling of the steel beams after the Cardington office demonstration test (Test 6) [18]. In this test, the maximum deflections of unprotected steel beams reached 640 mm and the beam temperatures reached 1150°C under a total fire load density of 46 kg/m<sup>2</sup>. As can be observed from the figure, the web and bottom flange of the beam experienced severe local buckling near the beam-end due to the deterioration of steel material under high temperature and the increase of fire-induced internal forces. Additionally, the local buckling is also induced by the beam-end restraint to thermal expansion, which causes large

compressive stresses at the beam-ends. Furthermore, the demand of beam-to-column connections is still important to the structural fire safety. Fig.2 (b) shows the connection failure in Cardington fire test (British Steel Test 2: Plane frame test) [18]. The connected plate or the bolt fracture is usually the major failure mode for beams in fire[19]. It means that the beam-end of the ordinary beam is the key zone of bearing higher combination of fire-induced fires and is the weakened section during the structures exposed to fire.

## **2.2 Fire-induced internal forces**

In ambient-temperature design, steel beams are designed to resist bending moment and shear. In fire, a steel beam experiences completely different loading (large axial forces and bending moments), as well as large deflections. Axial compression and bending moments can be caused by the restraint to thermal expansion and thermal bowling; axial tension and bending moments can be resulted from the large deflection of the beam, due to the degradation of mechanical properties of steel at high-temperatures.

Subject to fire, the axial forces in an axially restrained beam usually undergo three stages, as shown in Fig.3 [20]. During initial heating (shown as the Thermal Expansion Phase in this figure), the beam expands (or intends to expand) because of continuous heating, producing an additional compressive axial force and bending moment due to the effect of end-restraints. Hence, the connected elements (column and connection) could experience large deformation or fracture, causing progressive whole building collapse, as exemplified by the collapse of the World Trade 7th building [21] in the New York City. As illustrated in Fig. 3, the compression starts to decrease (Quasi-Catenary Phase in this figure, starting from  $T_a$ ), as the beam softens and deflects with increasing temperature. The compression reverses to tension when the beam deflection is large enough (Catenary Phase in this figure), and the beam and beam-to-column connection need to be able to resist the large catenary tension force at this stage.

The mid-span deflection limit,  $\text{span}/20$ , given in EC3 [22], is sometimes used as a 'failure' criterion when evaluating the safety and fire resistance of steel beams, in particular in structural fire engineering analytical design. In fire, the increase in beam deflection is mainly caused by the reduced beam stiffness and strength. When steel temperature is high enough, the flexural resistance of the beam falls below the applied load; tensile fracture could initiate from either the bottom flange of the mid-span of the beam or at the beam-to-column connections[23].

### **3. Performance of RBS beam in fire**

For H-section universal beams, the bending resistance is mainly provided by flanges (the web mainly provides shear resistance). In fire, the whole cross-section of the beam is required to bear the compression during the Thermal Expansion Phase (as illustrated in Fig. 3) as well as tension during the Catenary Action Phase. Additionally, the beam-ends also need to resist the bending moments caused by beam deflection (resulted from the loss of flexural stiffness at high temperature and from thermal deflections).

However, the behaviour of RBS beams, when exposed to fire, may be very different from that of ordinary beams. The RBS zone has significantly lower stiffness than that of the rest of the beam; therefore, it usually experiences high stress concentration. The response of the weakened RBS region to the additional internal forces induced by fire, as addressed in Section 2.2, could be very different from that of a normal beam. This has not been systematically investigated and a numerical study on this is presented in this paper.

#### ***3.1 High-temperature FEA structural analysis***

The static implicit solver of ABAQUS [24] has been used in the numerical modelling presented in this paper. A 7200 mm length beam (UB 406 × 140 × 46 [25]) connected to two rollers and restrained by the axial spring and the rotational spring( which were simulated in ABAQUS by using Spring element) at the beam ends, as illustrated in Fig.4, was used as the control model in this study. The geometrical

dimensions of the RBS zone of this control model were determined according to EC8 [8]. The design requirements given by FEMA-350[9] were employed for the parametric study on RBS-zone dimensions. Table 1 summarizes the design recommendations on RBS dimensions given by EC8 and FEMA-350.

The physical loading, 64.7kN (load ratio = 0.5; referred as LR5 hereafter) was adopted. The load ratio is defined as the ratio of applied bending moment to the bending moment resistance of the beam at ambient temperature.

### **3.1.1 Model setup**

The axial and rotational restraints provided by the columns to the beam-ends were modelled by the 1D linear spring element (Spring1) of ABAQUS at the cross-sectional origin. Multi-Point Constraints/beam (MPC/beam), a relationship between degrees of freedom in one or more nodes, was defined at the two supported ends of the steel beam models so that it can be modelled as the pinned supports at the MPC master node( at the cross-sectional origin). The type of MPC/ beam provides a rigid beam effect between the master node and the cross-section to constrain the displacement and rotation at the master node to the displacement and rotation at the cross-section. The stiffness of the rotational and axial springs are calculated as suggested by Dwaikat and Kodur [20], as illustrated in Fig. 5.

In order to reduce the number of elements and nodes in the finite element models, the steel beam was modelled symmetrically with 3D shell element (S4R), whose length was half of the beam.

Grade S355 steel, with yield strength of 355 N/mm<sup>2</sup> and Young's modulus of  $2.00 \times 10^5$  N/mm<sup>2</sup> at room temperature [25], was used for the model. The mechanical degradation of steel at elevated temperatures given by EC3[22] (as shown in Fig.6 and Fig.7) was applied. The thermal expansion coefficient for steel was  $1.4 \times 10^{-5}$  m/°C. The specific heat and thermal conductivity of steel were both temperature dependent and were determined according to EC3, as listed in Table 2.

The metal damage index of ductile criterion and shear criterion was employed in ABAQUS. The model assumes the damage starts when the specified equivalent plastic strain at the onset of damage is reached at point *c*, shown in Fig.8. The damage evolution, which is characterised by the progressive degradation of the material stiffness, was also defined, usually the ultimate strain of steel be set at point *d* (Fig.8). Once the fracture strain is reached, the damaged elements will be deleted from the model. The specified equivalent plastic strain and the ultimate strain, depending on the temperature[26], are defined as Table 3.

The analysis was divided into two steps, in which the physical loading was applied firstly and then the steel temperatures increased. Newton-Raphson method was adopted with a dissipated energy fraction of 1E-10; this value was chosen to achieve an optimum between computing efficiency and accuracy.

An amplitude of  $h/400$  of the first mode was assigned to the nodal displacements that served as the initial geometric imperfection of the arch models, in which  $h$  was the height of the cross-sections of the beam models.

### ***3.1.2 Fire scenarios considered in the models***

Different fire curves (temperature-time relationships) significantly affect the structural responses to fire. The ISO 834 Standard Fire Curve [27] is widely used in assessing the structural behaviour of isolated members in furnace tests. However, it bears little relationship with real fires. The temperature-time relationship of compartment fires is related to fire load, ventilation, compartment area, etc., none of which has been considered by the standard fire curve. Parametric fires given by EC1[28], considering the effects of compartment size, fuel load density, ventilation conditions and the thermal properties of compartment walls and ceilings, provide a simplified representation of natural post-flashover compartment fires for use in structural fire design.



The paper chose four types of fire curves, which hope to dispel the effects of the real fire in study. Since this analysis does not address any particular fire compartment, one parametric fire which is close to the standard fire was chosen, and two other parametric fires with higher degrees of ventilation (other parameters remain unchanged) were also employed, as shown in Fig. 9.

### ***3.1.3 Temperature distribution determined by heat-transfer analysis***

Thermally protected by the concrete slab, the top flange of a beam is usually cooler than the beam web and bottom flange; and this non-uniform temperature distribution within the beam cross-section results in different structural behaviour and internal force distribution compared to those of uniformly heated beams [16].

There has some literatures provided the suggestions on the non-uniform temperature distribution in steelwork sections [ e.g. 17]. Obtaining from tests is a direct way to ascertain the temperature distribution. However, the cases, including the fuel combustion, the geometric dimension of beam section and the heat insulation up the upper flanges, will limit the experimental temperature distribution to be used in a particular condition, not as the reference for others extensively.

The heat transfer analysis of ABAQUS was used to predict the temperature distribution within a beam cross-section, which was used as input for the high-temperature structural analysis. The ABAQUS diffusive element (DS3) was used in this heat transfer analysis, considering thermal radiation, thermal conductivity and specific heat (as illustrated in Section 3.1.1). The convection coefficient was  $25 \text{ W}/(\text{m}^2\text{K})$  as air natural convection and the radiant coefficient was 0.75. The Stefan-Boltzmann constant was  $5.67 \times 10^{-8} \text{ m}^2\text{K}^4$ . The results of heat transfer analysis of the model (as shown in Fig. 5) are plotted in Fig.10. Additionally, the steel temperatures induced by these four fire curves are also calculated by using the predicted approach in EC3: Part 1-2 as a comparison.

### **3.2 Model validation and sensitivity analysis**

The model was validated against experimental results. An unprotected restrained beam, tested by Li *et al.* [29], was used in this validation. The tested steel beam (4500 mm long and of section H250 × 250 × 8 × 12 [30]) was connected to two steel columns (1860 mm high and of section H300 × 300 × 16 × 25 [30]). Two pointed loads, 130kN, were applied at the trisection points of the beam length. The top flange of the beam was thermally protected by ceramic fibre blanket, for which the thicknesses were 10 mm. Q235B ( $f_y = 271$  MPa) steel was used for the beam and Q345B ( $f_y = 331$  MPa) steel was used for the columns.

The test fire curve and the measured steel temperature are plotted in Fig.11, including the validation of heat-transfer analysis by using ABAQUS. In the numerical model, the top flange of the beam was thermally protected as well. The thermal radiation, thermal conductivity and specific heat were determined according to EC2:1-2 [31]. Due to the lack of the furnace parameters of the test, the results of the heat transfer analysis are slightly higher than that of the test, but the gap between the numerical analysis and the test could be accepted. And the methods of the heat transfer analysis could be implemented in the following study.

This test was simulated as shown in Fig. 12a and Fig. 12b. The axial and rotational restraints, provided by the columns to the beam-ends, were modelled as described in Section 3.1.1. The spring stiffness of the axial spring (68.3 kN/mm) and that of the rotational spring (76 kNm/mrad) were calculated as described in Section 3.1.1.

The agreement is satisfactory overall, with the numerical results slightly overestimating the transition temperature from compression to tension in the beam. The reason is that the columns were affected under the high temperature in test, while they are replaced by Spring1 elements in the numerical simulation, which could not reflect the stiffness deterioration of columns in practice.

Three mesh sizes, 10 mm, 20 mm and 30 mm, were adopted in the mesh sensitivity analysis. The model, meshed by 20 mm, saves 26% of the running time compared to the model meshed by 10 mm. The results indicated that the mesh 20mm is appropriate and so it is used in the following analysis. The validity of the model setup, such as element type, material properties, mesh size and contact properties should not be affected by the various fire curves and imposed load levels adopted in the following parametric studies.

#### **4. Parametric studies**

##### ***4.1 Effect of fire curves***

In this section, the effects of fire curves on the performance of the RBS beam (control model) are discussed. The stiffness of the end restraints, simulated by axial and rotational springs, were calculated as described in Section 3.1.1, based on the configurations of the connected columns (UC 254 × 254 × 132 of 3.6 m height); the stiffness of the axial spring is 48.6 kN/mm and that of the rotational spring is 13.1 kNm/mrad. The applied load ratio is 0.5.

Fig.13 shows the development of the mid-span deflections and beam-end reaction axial forces over time of the model subject to different fire curves. The behaviour of the beam is controlled by the beam configurations and steel temperature and so at certain steel temperature, the mid-span deflection and beam-end axial forces were identical for all four cases. The fire resistance periods of the four cases are however different due the various time-temperature relationships used.

All models fail (defined as when strain exceeds the fracture strain in Table 4, as described in Section 3.1.1) at the RBS zone and their mid-span deflections at failure are all close to span/20. Under the fast parametric fire, the model experiences large deflection after only two minute due to the fast heating. On the contrary, the model exposed to Standard Fire has the longest fire resistance period among the four cases, due to the slower heating rate of the Standard Fire compared to the other fire curves. Fig. 13 (b) shows that, in all four cases, the beam experiences axial compression during initial

heating as well as catenary tension at higher temperatures when the beam weakens and loses its flexural stiffness. The maximum compressive and tensile forces of all cases are identical as they are controlled by the section size and steel temperature.

Compared with the ordinary beams (OB group), the effect of the cutting profile of the beam flanges is more significant on the fire performance of the connection model exposed to the slow-parametric fire and the standard fire, due to the fire speed and the reactive speed of the models. Considering the decay stage in parametric fire curves, this paper chose the slow-parametric fire as the main fire curve during the following study.

#### ***4.2 Influence of beam-end restraints***

The restraints at the beam-ends would influence the high-temperature performance of beams in fire, due to the variation of internal force distributions caused by the beam-end restraints. This study uses three levels of restraint (modelled by translational and rotational springs) to investigate the effects of the beam-end restraint.

The restraint stiffnesses based on three different column sections (UC 254 × 254 × 132, UC 305 × 305 × 137 and UC 356 × 368 × 153) were adopted. The axial stiffness and rotational stiffness are 48.6kN/mm and 13.1 kNm/mrad for UC 254 × 254 × 132(S1); 70.9kN/mm and 19.1 kNm/mrad for UC 305 × 305 × 137 (S2) and 104.9 kN/mm and 28.3 kNm/mrad for UC 356 × 368 × 153 (S3), which were assigned to the spring elements (Spring1) in ABAQUS. The dimensions of the models are identical to those of the control model (Fig.4). The slow parametric fire and load ratio = 0.5 were adopted. Additionally, ordinary beams (OB) without RBS, with the same end restraints were also considered for comparison.

The performance of the RBS and OB models is plotted in Fig.14. As restraint stiffnesses increase, the mid-span vertical deflection increases, due to the increased restraint to thermal expansion which increases the compressive axial force in the beam further increasing its deflection during initial

heating. The beam-end tensile force in the catenary tension phase at very high temperature is not affected by the stiffnesses of the beam-end restraints, due to the very low stiffness of the beam itself compared to the connected columns, which stays cool. In all three cases, the beam fails by fracturing the RBS zone. Because the lateral restraints were assigned to the top flanges of all models, the global buckling and local buckling (non-RBS zone) did not occur during the numerical analysis. Hence, only the failure process of the RBS zone is shown as Stage A-D of Failure Mode 1 in Table 4. The failure deflections of the three case are all close to  $\text{span}/20$ , which are not influenced by the level of end restraints. However, the fire resistance period considerably shortens with higher restraint stiffnesses, since comparing with the low restraint case (1) the beam end bending moment is higher and (2) the difference in capacity between the RBS zone and the connected column is larger. RBS beams were initially introduced to relieve the beam-end moment for earthquake design and this works as well in fire conditions; comparing with the OB models (Fig. 14), the RBS models survived longer fire resistance periods. This beneficial effect due to the high rotational capacity of RBS is more significant when the end restraint is stiffer, which increases the beam-end bending moment and increase the demand on the moment capacity of the beam. The RBS beam fails at the RBS zone, whereas the OB fails at the beam end (Failure Mode 3 in Table 4). With the same beam-end restraints, the mid-span deflection of the RBS beam is larger than that of OB before failure, due to the RBS's larger rotational capacity.

In general, the fire resistance period of the model under the low parametric fire is longer under lower end restraints or when the beam has RBS. This effect of RBS on extending the fire resistance period is more signification when the end restraints are higher.

#### ***4.3 Effect of the cutting profile of RBS under different load ratios***

EC8 provides one type of RBS geometrical profile and the FEMA-350 allows a range of cutting dimensions of RBS. Five cutting profiles for UB 406 × 140 × 46 recommended by these two codes are summarised in Table 5. The RBS dimensions are dependent on three parameters: (1) the distance from the edge of the RBS zone to the beam-end,  $a$ ; (2) the cutting length of RBS zone,  $b$ ; and (3) the distance from the centre of the RBS zone (the narrowest section in the beam) to the beam-end,  $d$ . The effect of the cutting profiles on the fire performance of the RBS beam is presented in this section. Model RBS-1 is the control model (UB 406 × 140 × 46, span 7.2 m, with the axial restraint = 48.6kN/mm and the rotational restraint = 13.1 kNm/mrad) adopted in the previous sections. The slow parametric fire is again used in this parametric study and four load ratios (0.3, 0.5, 0.7 and 0.9) are adopted. The ordinary beams with the same end restraints as for the RBS models are also considered for comparison.

Figures 15 and 16 show the mid-span deflections and the beam-end axial reaction forces of the models with different cutting geometrical sizes. Under the smallest load ratio (0.3), all RBS models experienced very similar mid-span deflections and the beam-end reaction forces. As the load ratio increases, the differentiation between the models becomes more obvious; in other words, the influence of RBS geometrical profile on the beam's fire performance is more significant under high load ratios.

In terms of beam-end axial forces (Fig. 16), during the initial heating stage, the compressive force in the beam is rarely influenced neither by the load ratio nor by the cutting dimensions. After the initial heating stage, the effect of the load ratio and that of the RBS dimensions on the beam-end axial forces is more significant. As load ratio increases, the fire resistance periods of all RBS models shorten; the models get into catenary action phase earlier and experience higher catenary tensile forces. The failure modes of all RBS models are identical (Failure Mode 1, Table 4), except Model RBS-3 (of the largest cutting length) experienced lateral torsional buckling (Failure Mode 2, Table 4), which was also observed in ambient-temperature loaded tests [32].

All RBS models (except RBS-4) survive longer fire resistance period than the ordinary beam (OB) model. Since the RBS zone of RBS-4 is the closest to the beam end, it experiences the largest bending moment and shear force and hence the beam has the lowest fire resistance, compared to the other cutting profiles. It can be observed that RBS-4 fractures at the Quasi-Catenary Phase.

The fire resistance of RBS-2 is the second lowest among the five RBS model; it is only larger than that of the RBS-4. This is because RBS-2 has the shortest cutting length and so the lowest rotational ductility, which is needed to relieve the beam-end bending moment to avoid failure.

The performance of RBS-1, RBS-3 and RBS-5 are similar; they all fail by tensile fracture at the RBS zone during the Catenary Phase (Failure Mode 1, Table 4).

In conclusion, controlling the distance  $d$  from the RBS zone to the beam end and the cutting length  $b$  during the design of RBS beams is an effective way of achieving satisfactory fire performance. For the beam size analysed, the cutting length  $b$  suggested by EC8 and the distance  $d$  given by FEMA-350 based on the largest  $a$  ( $= 0.7 b_f$ ) will lead the most satisfying fire resistance.

## 5. Conclusions

This paper presents an investigation on the high-temperature performance of RBS beams, considering the effects of the geometrical size of RBS, beam-end restraints and fire time-temperature relationship. The following conclusions can be made based on the beam models analysed:

(1) The fire performance of the RBS beams and that of the ordinary beam, subject to the same beam-end restraints and to the same external loads, are similar under low end restraints and low load ratio (e.g. 0.3). As load ratio increases, the behaviour of RBS beam and the OB before cut differentiates from each other; RBS's enhanced rotational ductility compared to OB, leads to long fire resistance period;

(2) Under the different fire curves adopted, the fire resistance periods of the RBS models are influenced only by the heating rate. The internal forces and maximum deflections of the beams subject to different fire curves are identical, as they are controlled by the section size and steel temperature;

(3) Controlling the distance from RBS zone to the beam-end and the cutting length during the RBS beam design is an effective method of obtaining sufficient fire resistance. The cutting length proposed by EC8 and the distance from RBS zone to the beam-end suggested by FEMA-350 will lead to the best fire resistance.

It is recognised that further investigations are still needed before the above conclusions could be generalised and applied to all RBS beams subject to all loading conditions in all fire scenarios. For instance, a wider range of RBS beam sections should be analysed and the isolated effects of the axial and rotational restraints should also be investigated.

### **Acknowledge**

The research, in this paper, supported by Jiangsu Key Laboratory of Environmental Impact and Structural Safety in Engineering, China University of Mining & Technology. The authors would like to thank for its support of this area of research as one of the plan items of application and innovation, which is numbered as JSKL2014K02. Last, the authors appreciate the supported by China Scholarship Council (CSC: 201406425001).

### **Reference**

- [1] SAC. Interim guidelines: evaluation, repair, modification and design of steel moment frames. Emergency Management Agency, report no. SAC-95-02. 1995.
- [2] Roeder C, Foutch D. Experimental Results for Seismic Resistant Steel Moment Frame Connections. J Struct Eng 1996;122:581–8.
- [3] FEMA-267A. Interim Guidelines Advisory No.1: Supplement to FEMA 267. Federal Emergency Management Agency. 1997.



- [4] Chen S, Yeh C, Chu J. Ductile Steel Beam-to-Column Connections for Seismic Resistance. *J Struct Eng* 1996;122:1292–9.
- [5] Pachoumis DT, Galoussis EG, Kalfas CN, Efthimiou IZ. Cyclic performance of steel moment-resisting connections with reduced beam sections — experimental analysis and finite element model simulation. *Eng Struct* 2010;32:2683–92.
- [6] Sofias CE, Kalfas CN, Pachoumis DT. Experimental and FEM analysis of reduced beam section moment endplate connections under cyclic loading. *Eng Struct* 2014;59:320–9.
- [7] European Committee for Standardization(CEN). Eurocode 3:Design of steel structures,Part 1-8:Design of joints. EN1993-1-8,Brussels: 2005.
- [8] European Committee for Standardization(CEN). Eurocode 8:Design of structures for earthquake resistance,Part 3:Assessment and retrofitting of buildings. EN 1998-3,Brussels: 2005.
- [9] Federal Emergency Management Agency (FEMA). Recommended seismic design criteria for new steel moment frame buildings. FEMA-350, SAC Joint Venture Washington, DC; 2000.
- [10] ANSI A. Aisc 358–05 prequalified connections for special and intermediate steel moment frames for seismic applications. Chicago: American Institute of Steel Construction Inc.; 2005.
- [11] Newman G, Robinson J, Bailey C. Fire safety design: a new approach to multi-storey steel framed buildings. Ascot Berkshire (UK): SCI Publication; 2000.
- [12] Chung H-Y, Lee C-H, Su W-J, Lin R-Z. Application of fire-resistant steel to beam-to-column moment connections at elevated temperatures. *J Constr Steel Res* 2010;66:289–303.
- [13] Selamat S, Garlock ME. Robust fire design of single plate shear connections. *Eng Struct* 2010;32:2367–78.
- [14] Wang M, Wang P. Strategies to increase the robustness of endplate beam–column connections in fire. *J Constr Steel Res* 2013;80:109–20.
- [15] Lee C-H, Chiou Y-J, Chung H-Y, Chen C-J. Numerical modeling of the fire–structure behavior of steel beam-to-column connections. *J Constr Steel Res* 2011;67:1386–400.
- [16] Liu TCH. Effect of connection flexibility on fire resistance of steel beams. *J Constr Steel Res* 1998;45:99–118.
- [17] Pakala P, Kodur V, Selamat S, Garlock M. Fire behavior of shear angle connections in a restrained steel frame. *J Constr Steel Res* 2012;77:119–30.
- [18] The Cardington and Broadgate Fires. <http://911research.wtc7.net/mirrors/guardian2/fire/cardington.htm>.
- [19] Chen L, Wang YC. Methods of improving survivability of steel beam/column connections in fire. *J Constr Steel Res* 2012;79:127–39.

- [20] Dwaikat M, Kodur V. Engineering Approach for Predicting Fire Response of Restrained Steel Beams. *J Eng Mech* 2010;137:447–61.
- [21] NIST. Final Report on the Collapse of World Trade Center Building 7, Federal Building and Fire Safety Investigation of the World Trade Center Disaster. NIST NCSTAR 1A, USA: 2008.
- [22] European Committee for Standardization (CEN). Eurocode 3: Design of steel structures, Part 1-2: general rules-structural fire design. EN1993-1-2, Brussels; 2005.
- [23] Dai XH, Wang YC, Bailey CG. Numerical modelling of structural fire behaviour of restrained steel beam–column assemblies using typical joint types. *Eng Struct* 2010;32:2337–51.
- [24] Manual AU. Abaqus 6.12. Providence, RI, USA: Dassault Systèmes Simulia Corp.; 2012.
- [25] European Committee for Standardization (CEN). Eurocode 3: Design of steel structures, Part 1-1: General rules and rules for buildings. EN1993-1-1, Brussels: 2005.
- [26] Yu H, Burgess IW, Davison JB, Plank RJ. Tying capacity of web cleat connections in fire, Part 1: Test and finite element simulation. *Eng Struct* 2009;31:651–63.
- [27] International Standards Organisation. ISO 834-1: Fire-resistance tests-Elements of building construction. General requirements. 1999.
- [28] European Committee for Standardization (CEN). Eurocode 1: Actions on structures, Part 1-2: General actions-Actions on structures exposed to fire. EN1991-1-2, Brussels: 2002.
- [29] Li G-Q, Guo S-X. Experiment on restrained steel beams subjected to heating and cooling. *J Constr Steel Res* 2008;64:268–74.
- [30] Chinese standard (GB 2003). Code for design of steel structures. In: GB 50017-2003. Beijing. Chinese Plan Press. Beijing, China: 2003.
- [31] European Committee for Standardization (CEN). Eurocode 2: Design of concrete structures, Part 1-2: General rules-Structural fire design. EN1993-1-2, Brussels: 2004.
- [32] Ohsaki M, Tagawa H, Pan P. Shape optimization of reduced beam section under cyclic loads. *J Constr Steel Res* 2009;65:1511–9.

<Table>

Table.1 RBS cutting size given by EC8 and FEMA-350

Table.2 Thermal properties of steel

Table.3 The metals damage index of ductile criterion

Table.4. Fracture modes of models

Table.5. Geometrical sizes of RBS zone according to the EC8 and FEMA-350

<Figure>

Fig.1. RBS joints with circular-cut type (a) geometry of RBS joints; (b) location of plastic hinge in RBS zone; (c) bending moment capacity and design bending moment.

Fig.2. The local buckling and the fracture of beams in Cardington fire test [18]. (a) Cardington office demonstration test (Test 6); (b) Cardington British Steel Test 2: Plane frame test.

Fig.3. Axial force in a restrained steel beam exposed to fire.

Fig.4. Geometrical details of the control model: (a) geometrical size of the RBS beam model with boundary conditions; (b) geometrical size of the RBS zone according to EC8.

Fig.5. ABABUS model of the beam.

Fig.6. Stress-strain curves of structural steel at elevated temperatures

Fig.7. Reduction factors for Young's modulus and yield strength of steel at various temperatures

Fig.8. Typical uniaxial stress-strain response of a metal specimen with damage evolution.

Fig.9. Four different fire curves used in the numerical modelling.

Fig.10. Results of heat transfer analysis of the RBS models. (a) Parametric Fire-Fast; (b) Parametric Fire-Medium; (c) Parametric Fire-Slow; and (d) Standard Fire.

Fig.11. Test fire curve and temperature distributions in a beam section.

Fig.12 Relationship of mid-span deflection with time of model validation against test data. (a) Mid-span deflections; (b) Axial forces

Fig.13. Mid-span deflections and axial forces of RBS beam models and the ordinary beam model under different fire curves. (a) Mid-span deflections; (b) Axial forces

Fig.14. Performance of RBS models against to OB beam models with different beam-end restraints: (a) Mid-span deflections; (b) Fire-induced axial forces.

Fig.15. Mid-span deflections of RBS models with different cutting profiles against the ordinary beam

Fig.16. Fire-induced axial forces of RBS models with different cutting profiles against the ordinary beam

**Table1**

Table.1 RBS cutting size given by EC8 and FEMA-350

EC8, Part 3	FEMA350-2000 OMF, SMF
$a = 0.6b_f$	$a = (0.5 \text{ to } 0.7)b_f$
$b = 0.75b_d$	$b = (0.65 \text{ to } 0.85)b_d$
$c \leq 0.25b_f$	$c \leq 0.25b_f$
$r = (4c^2 + b^2) / 8c$	$r = (4c^2 + b^2) / 8c$

**Table 2**

Table.2 Thermal properties of steel [22]

	Value	Steel temperature
Specific heat, $c$ , (J/kgK)	$425 + 7.73 \times 10^{-1} \theta - 1.69 \times 10^{-3} \theta^2 + 2.22 \times 10^{-6} \theta^3$	$20^\circ\text{C} \leq \theta < 600^\circ\text{C}$
	$666 + \frac{13002}{738 - \theta}$	$600^\circ\text{C} \leq \theta < 735^\circ\text{C}$
	$545 + \frac{17820}{\theta - 731}$	$735^\circ\text{C} \leq \theta < 900^\circ\text{C}$
	650	$900^\circ\text{C} \leq \theta \leq 1200^\circ\text{C}$
Thermal conductivity, $\lambda$ , (W/mK)	$54 - 3.33 \times 10^{-2} \theta$	$20^\circ\text{C} \leq \theta < 800^\circ\text{C}$
	27.3	$800^\circ\text{C} \leq \theta \leq 1200^\circ\text{C}$

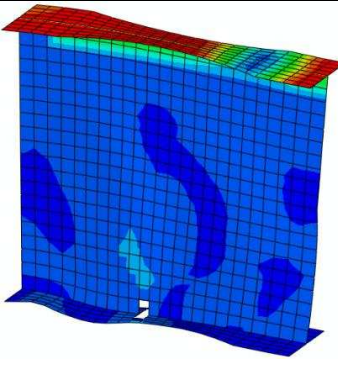
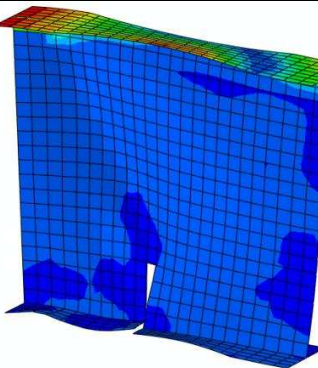
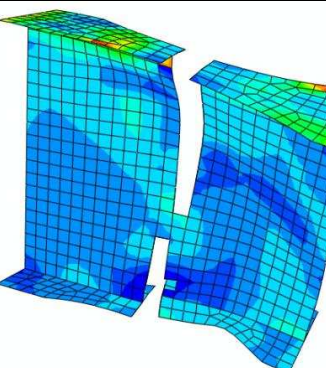
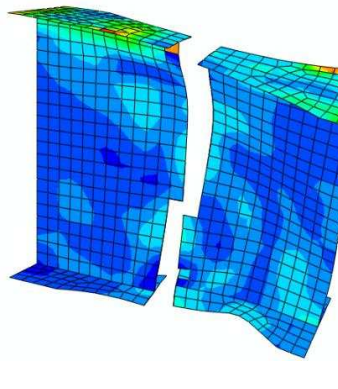
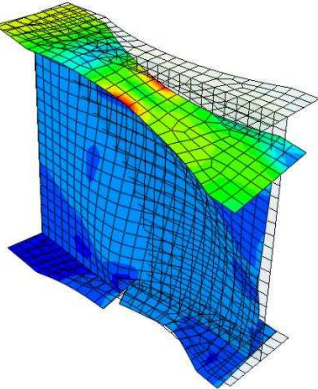
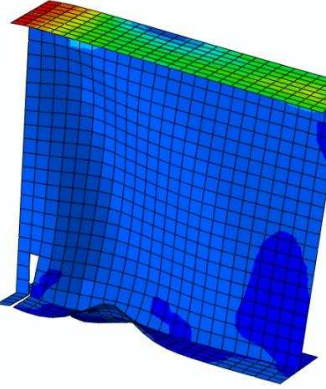
**Table 3**

Table.3 The metals damage index of ductile criterion [26]

Point <i>c</i>	Point <i>d</i>	Temperature
0.20	0.25	$T \leq 400^{\circ}C$
0.25	0.30	$T = 500^{\circ}C$
0.30	0.50	$T = 600^{\circ}C$
0.57	0.60	$T = 700^{\circ}C$

**Table 4**

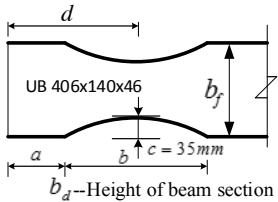
Table.4. Fracture modes of models

Failure Mode 1 – Stage A	Failure Mode 1 – Stage B	Failure Mode 1 – Stage
		
<p>The web fracture firstly under the combination of the internal forces and the fire-induced forces.</p>	<p>The fracture expands in the web and the bottom flange under the higher compression caused by the thermal expansion; and the extreme shear buckling occurs in the web.</p>	<p>The narrowest section at the RBS zone fractures under the tensile forces in the Catenary Phase.</p>
Failure Mode 1 – Stage D	Failure Mode 2	Failure Mode 3
		
<p>The weakened section departs fully.</p>	<p>For the RBS beam with the longer cutting length, the lateral instability is usually the major failure mode during the Quasi-Catenary Phase.</p>	<p>The ordinary beam fractures near to the beam-end usually under the higher combination of force, whose fire resistance is lower than the RBS beam's.</p>

**Table 5**

Table.5. Geometrical sizes of RBS zone according to the EC8 and FEMA-350

Models	Parameters		
	$a$ /mm	$b$ /mm	$d$ / mm ( $= a + b / 2$ )
RBS-1( EC8)	$0.6 b_f = 85$	$0.75 b_d = 300$	235
RBS-2	$0.73 b_f = 104$	$0.65 b_d = 262$	235
RBS-3	$0.46 b_f = 64$	$0.85 b_d = 342$	235
RBS-4	$0.5 b_f = 71$	$0.75 b_d = 300$	221
RBS-5	$0.7 b_f = 99.5$	$0.75 b_d = 300$	249.5



UB 406x140x46

$b_d$ --Height of beam section



Figure 1  
[Click here to download high resolution image](#)

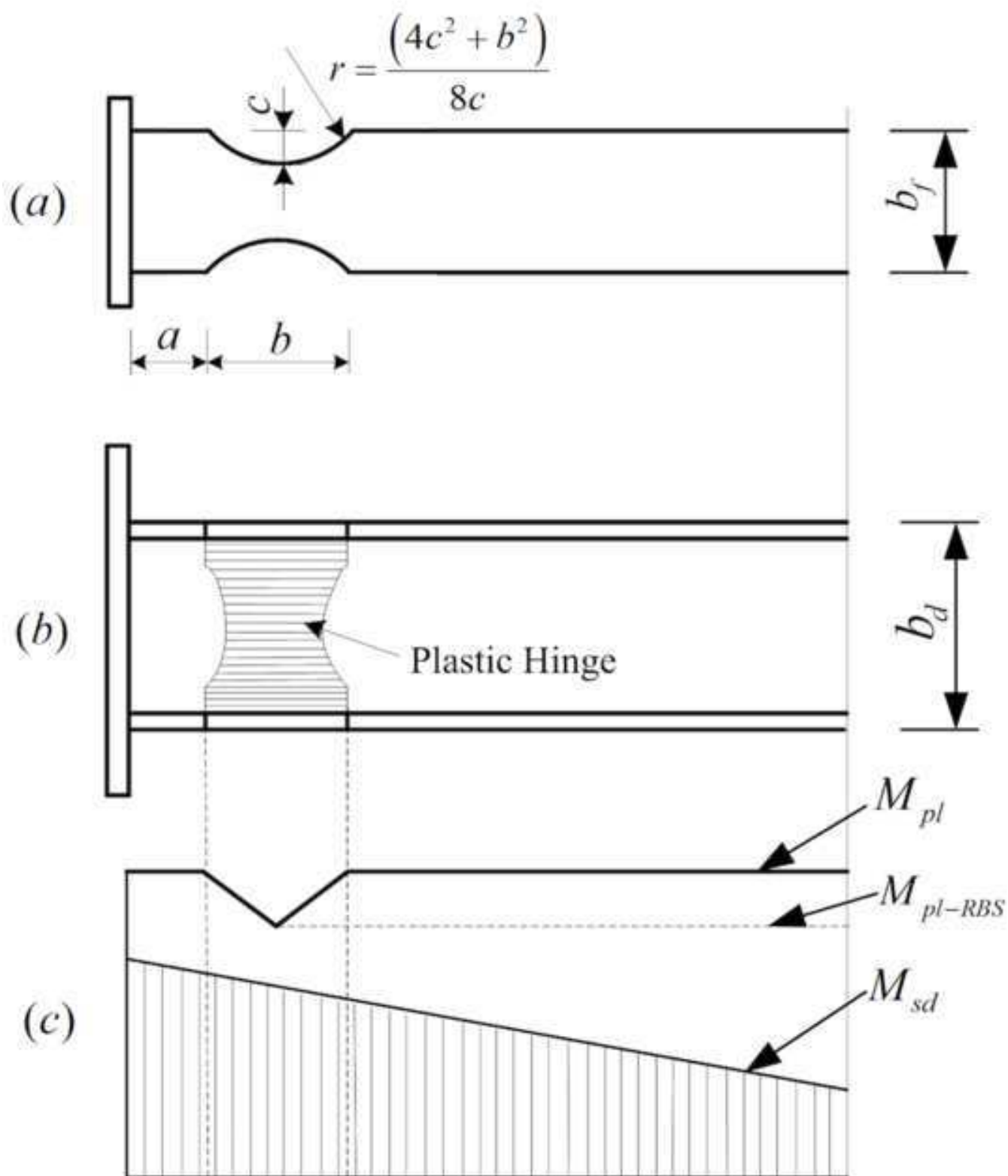
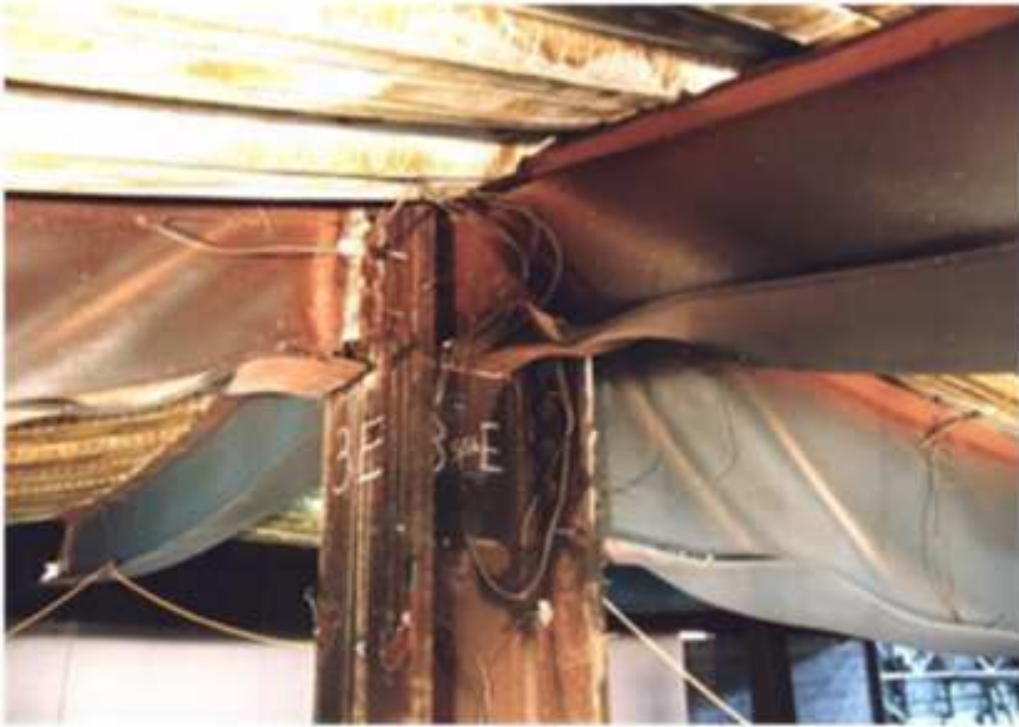


Figure 2  
[Click here to download high resolution image](#)



(a)



(b)

Figure 3

[Click here to download high resolution image](#)

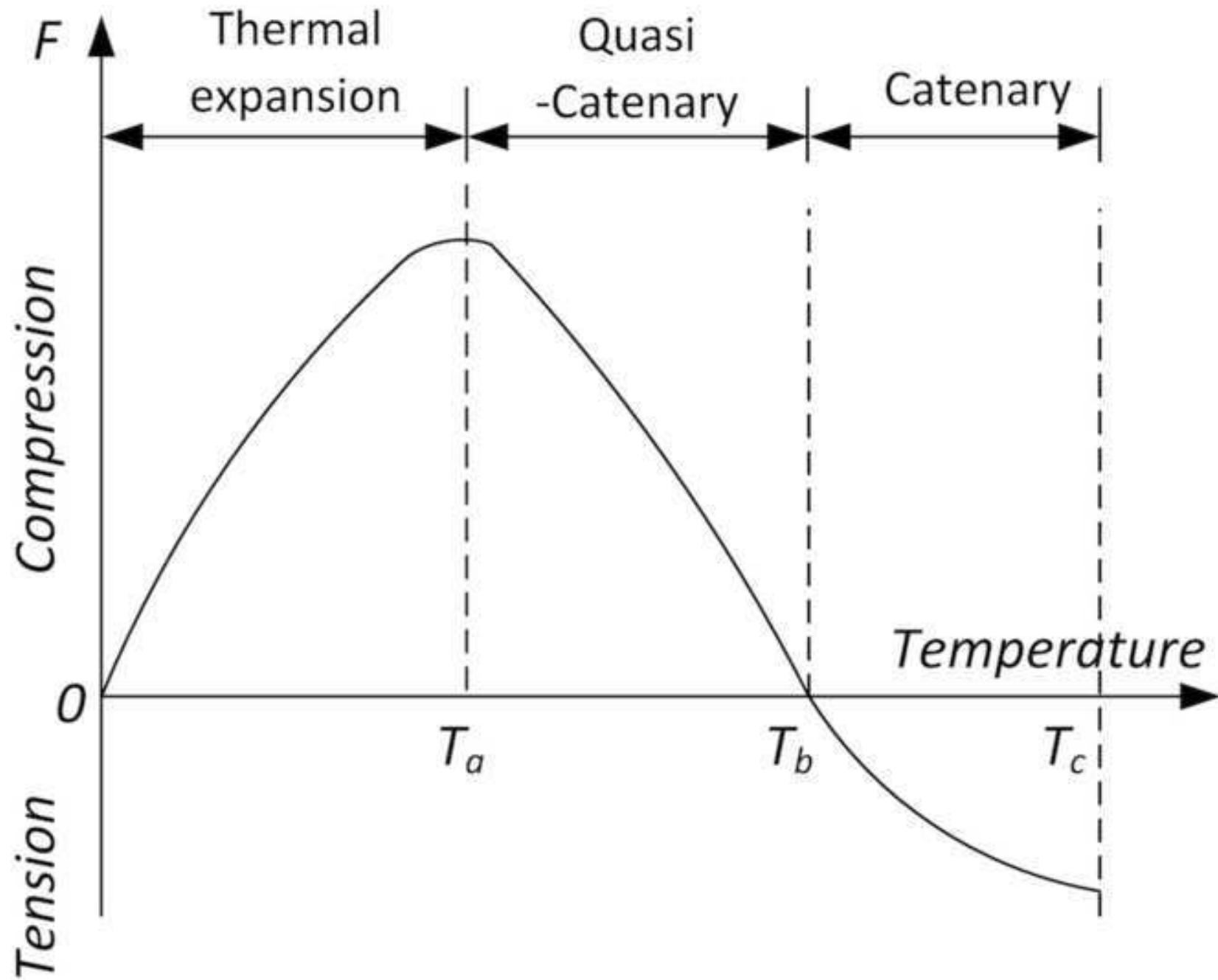
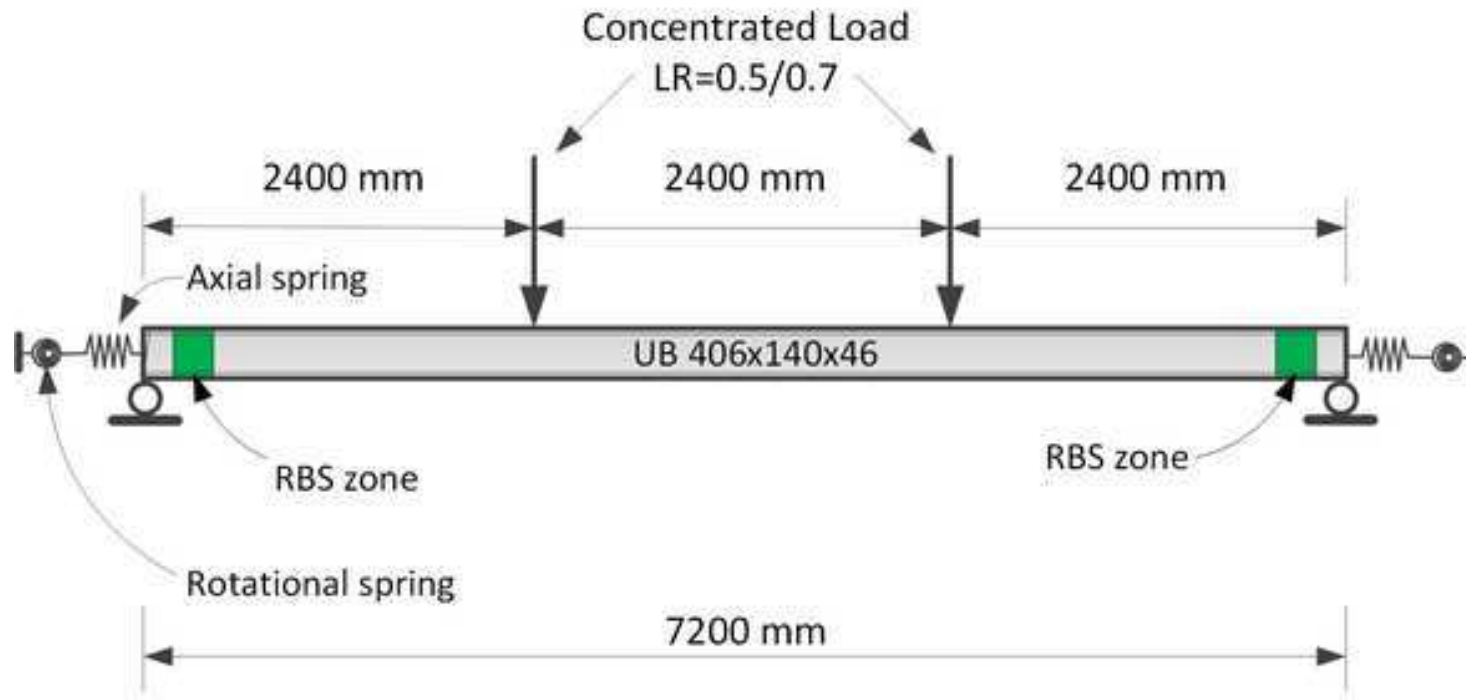
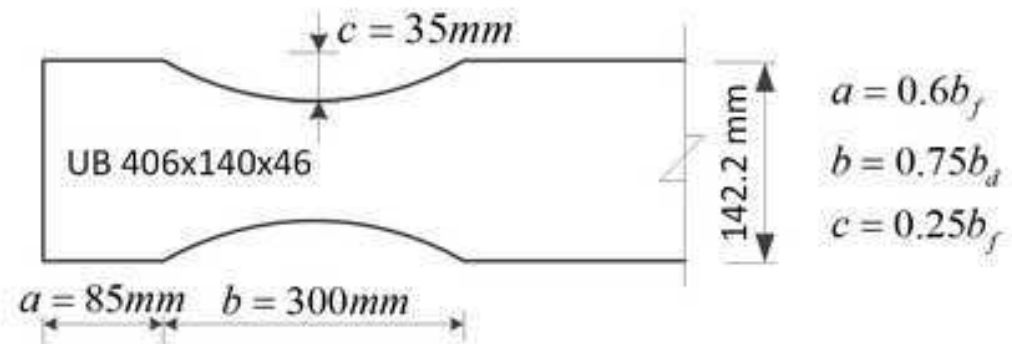


Figure 4

[Click here to download high resolution image](#)



(a) Geometrical size of the RBS beam model with boundary conditions



(b) Geometrical size of the RBS zone according to EC8 [8]

Figure 5

[Click here to download high resolution image](#)

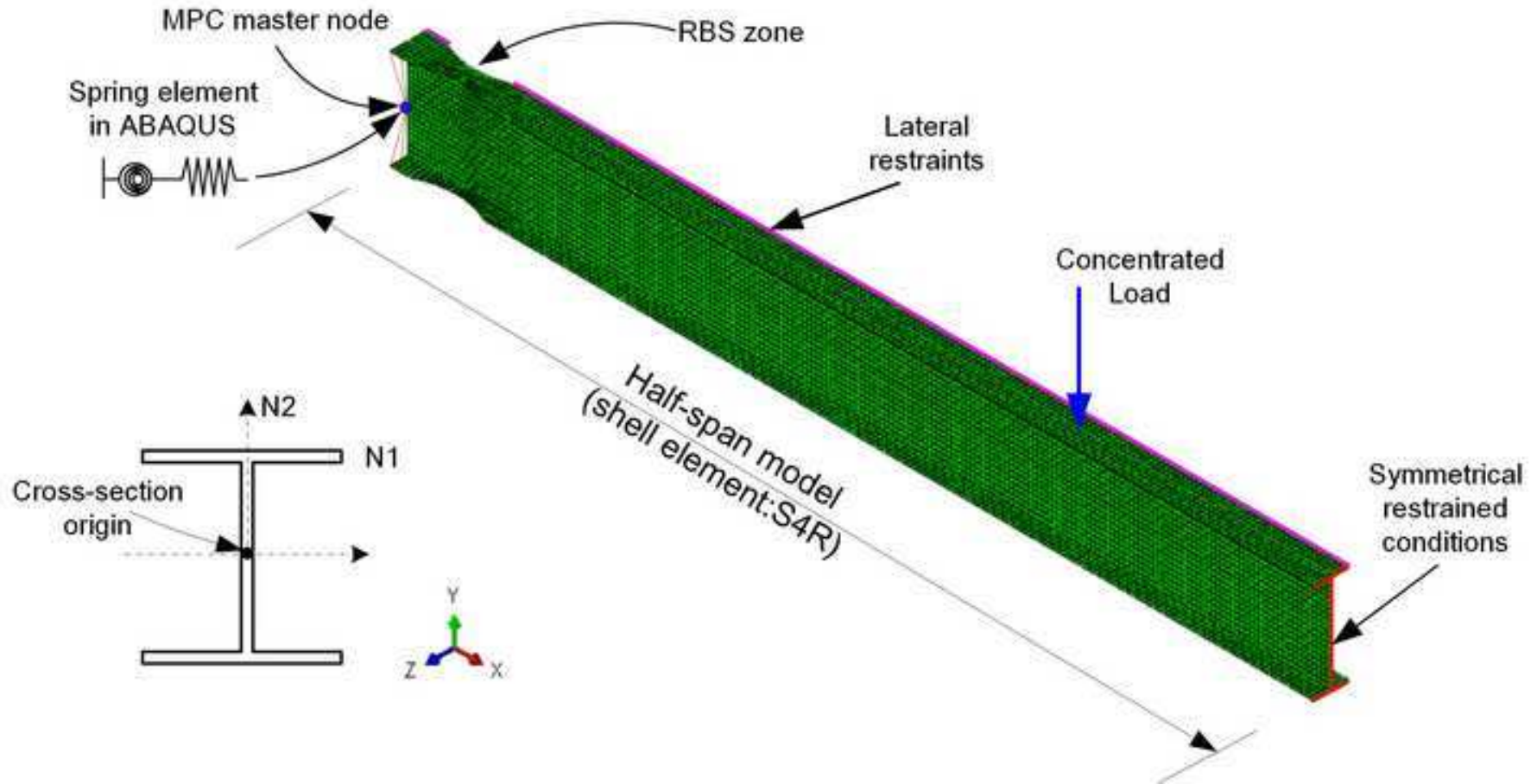


Figure 6

[Click here to download high resolution image](#)

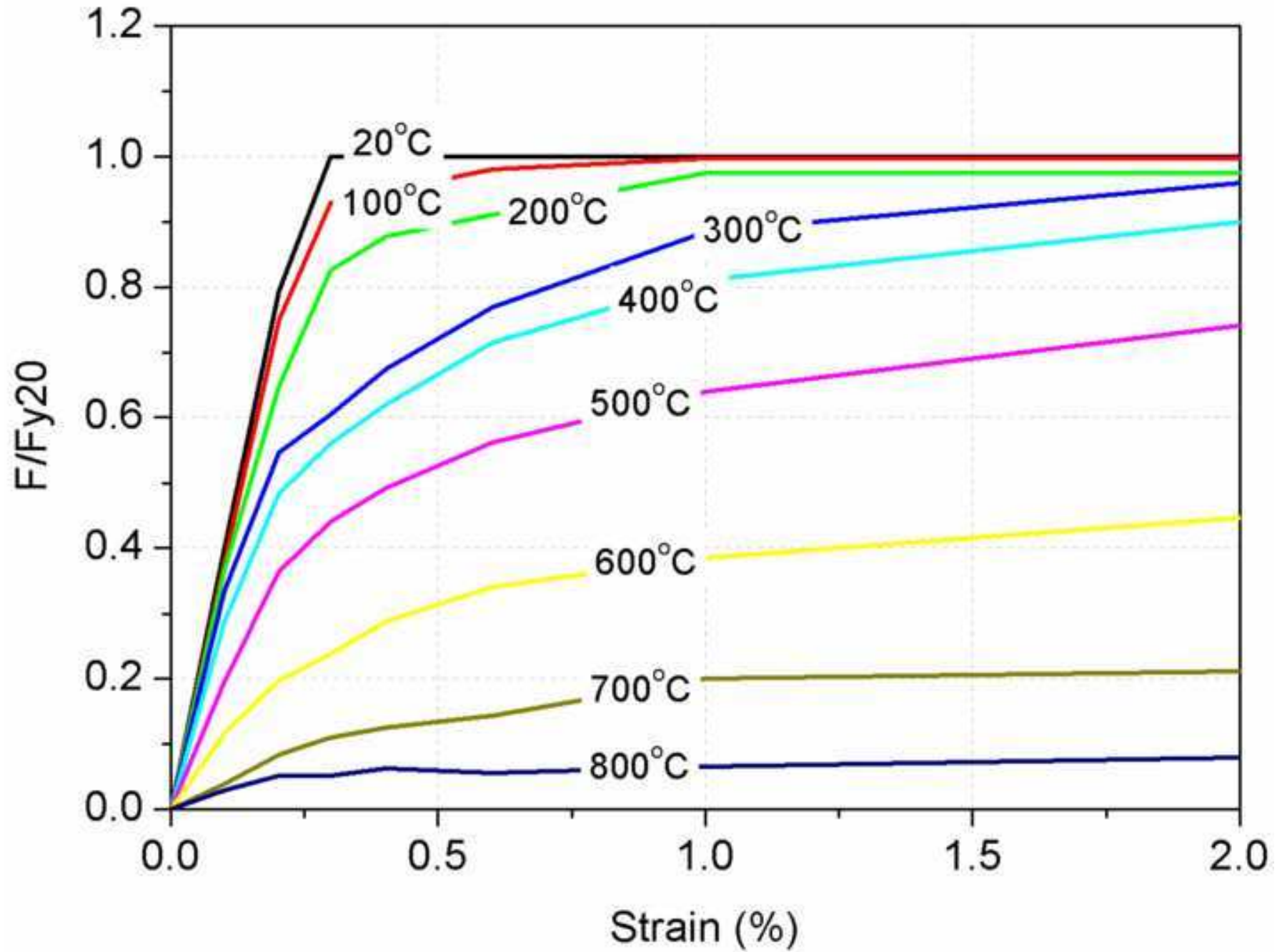


Figure 7

[Click here to download high resolution image](#)

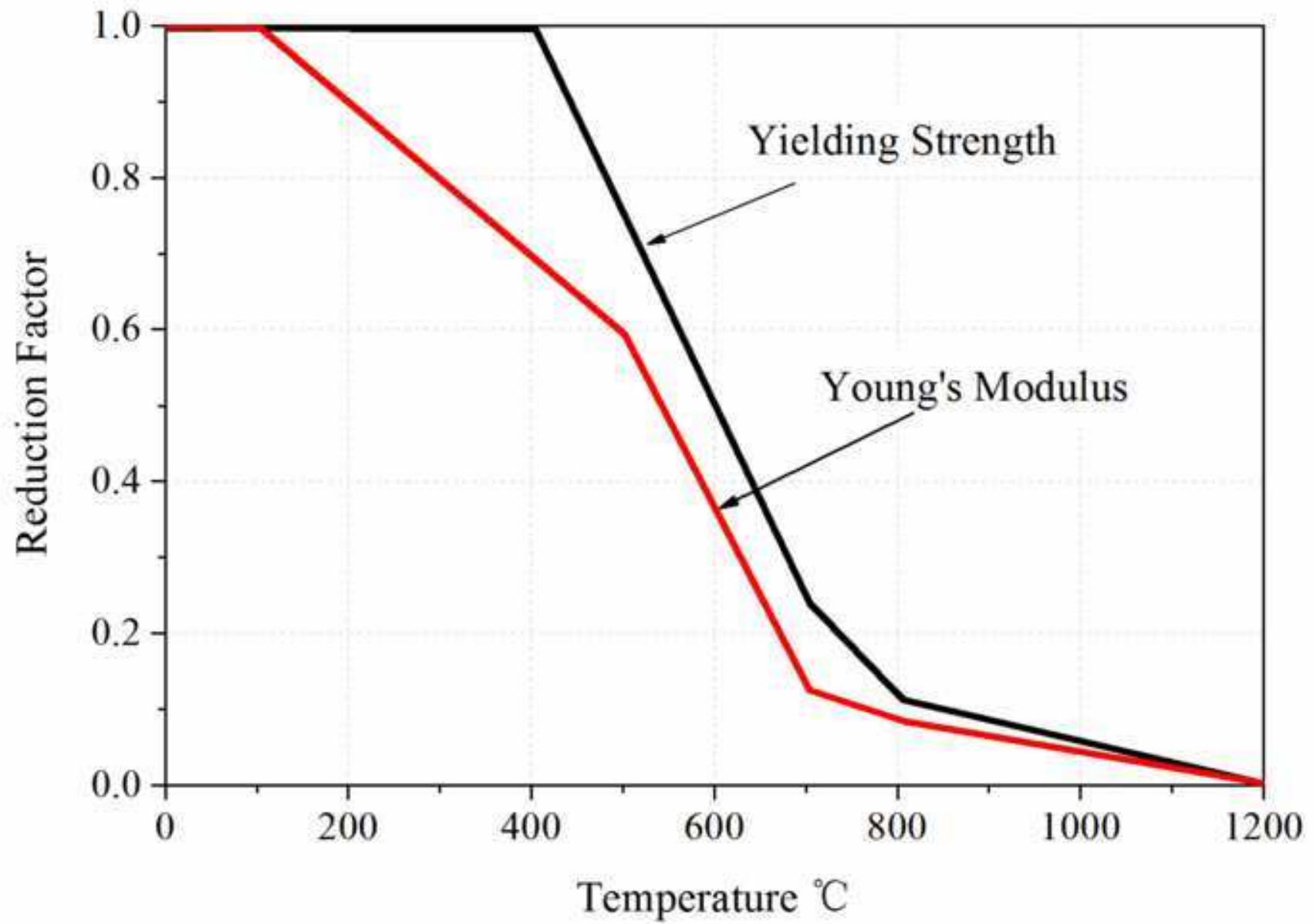


Figure 8  
[Click here to download high resolution image](#)

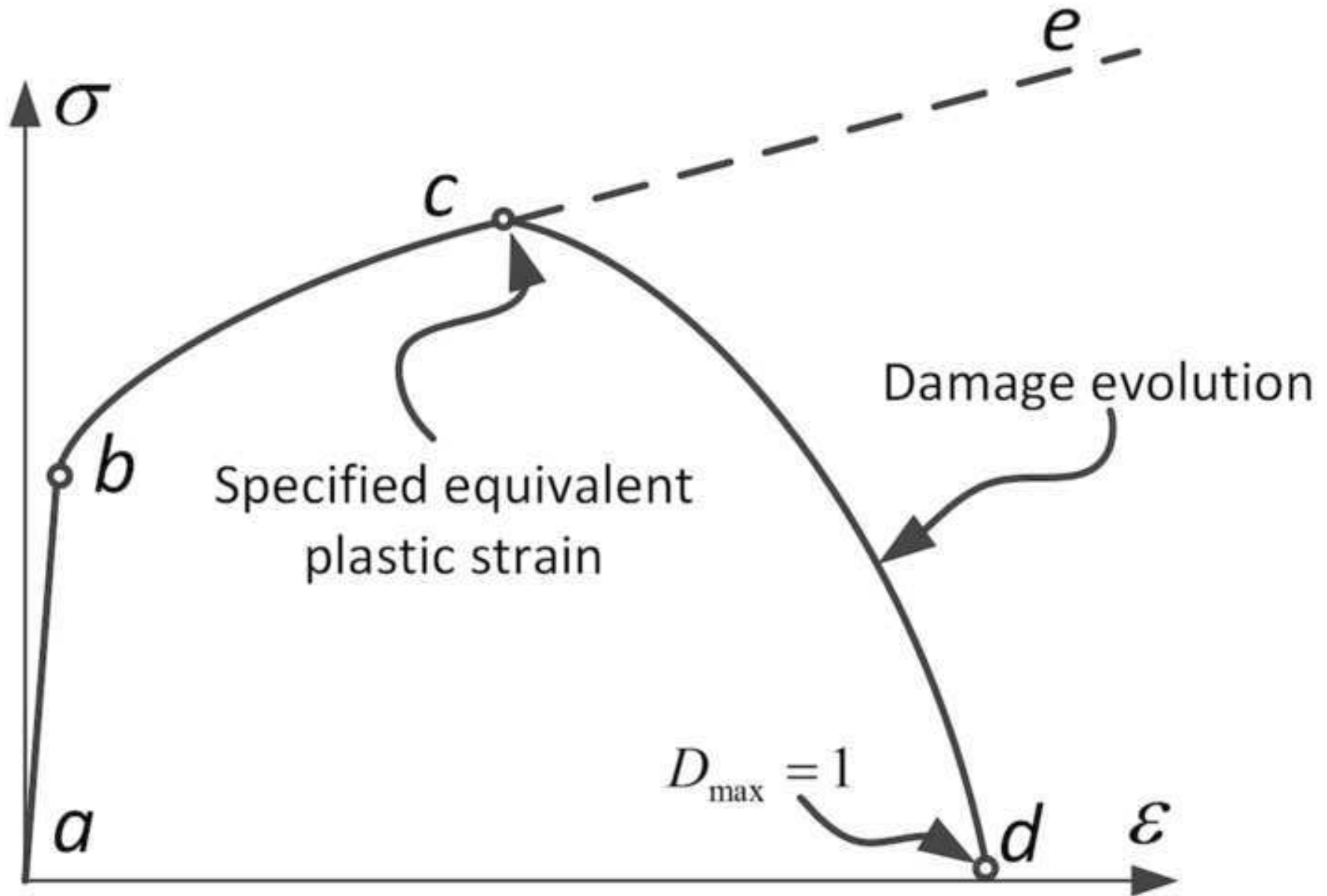




Figure 9

[Click here to download high resolution image](#)

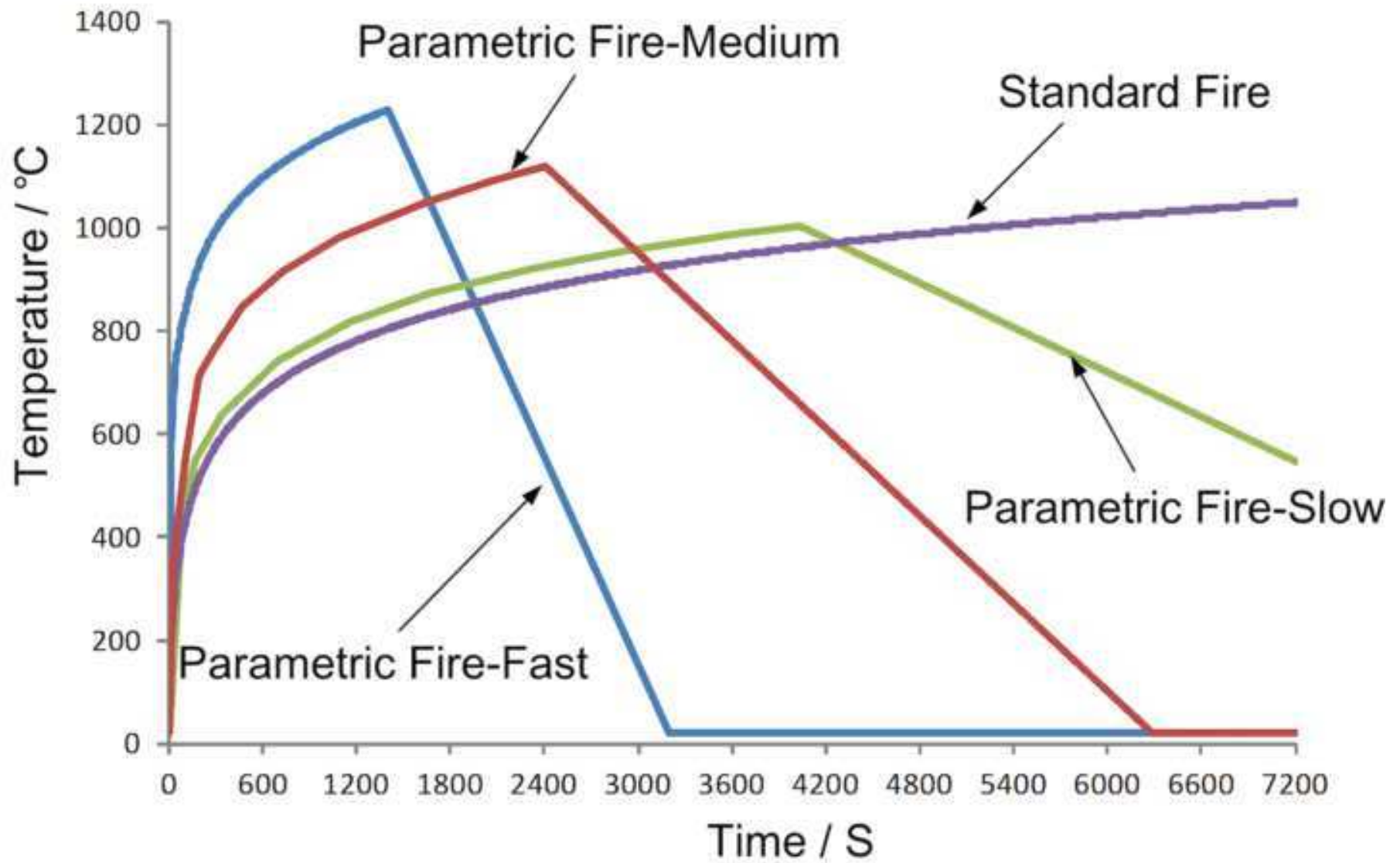


Figure 10a

[Click here to download high resolution image](#)

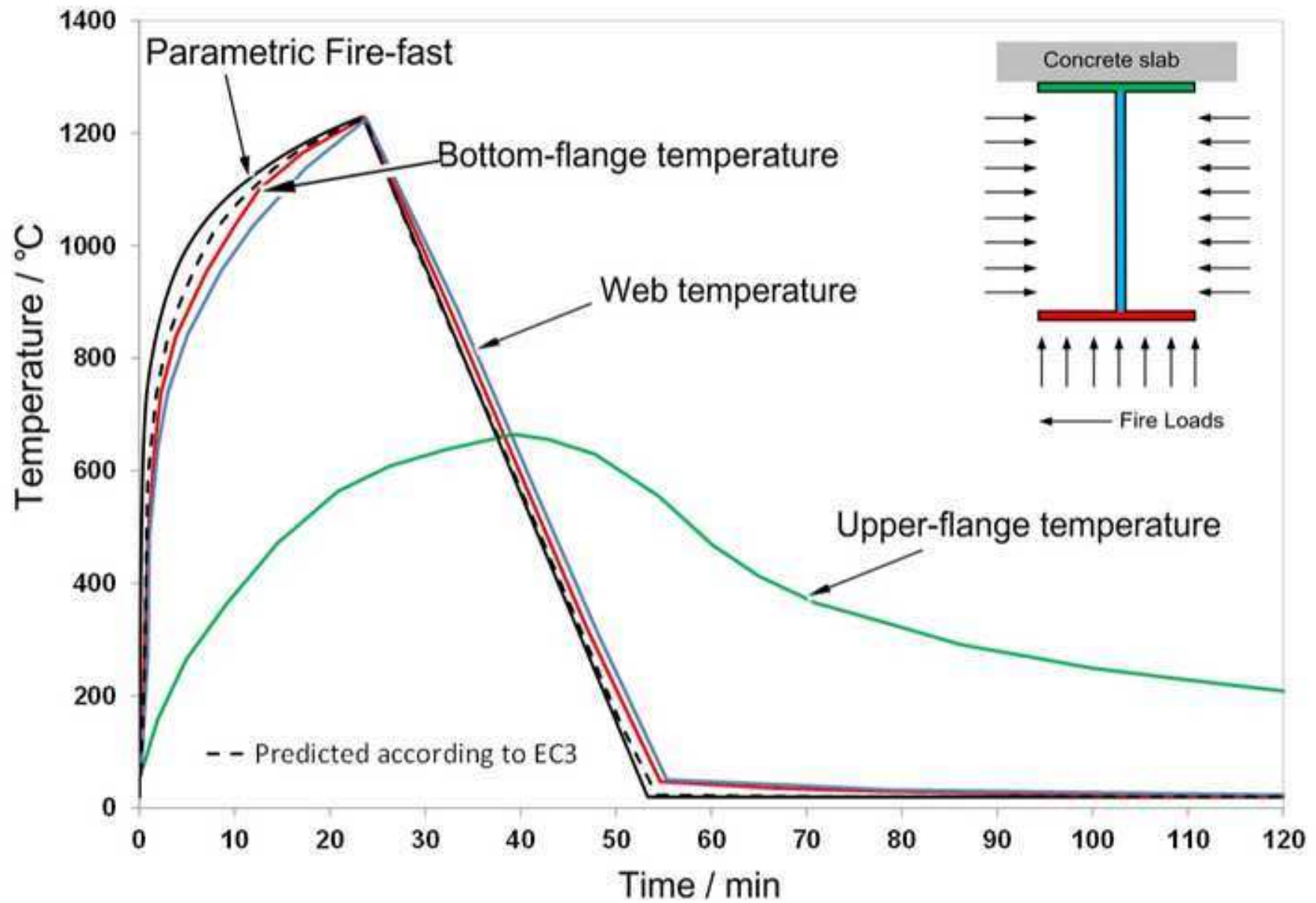


Figure 10b

[Click here to download high resolution image](#)

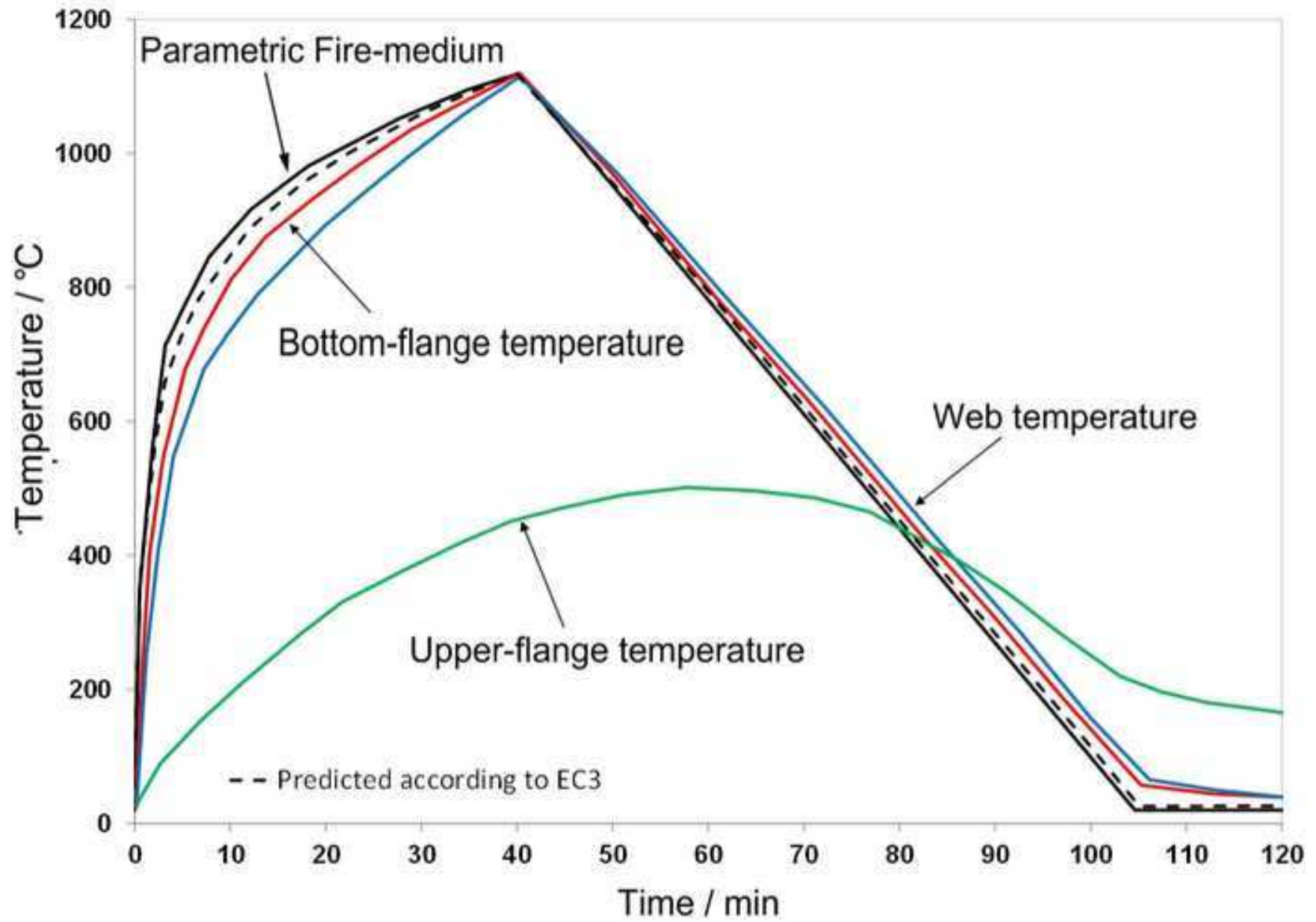


Figure 10c

[Click here to download high resolution image](#)

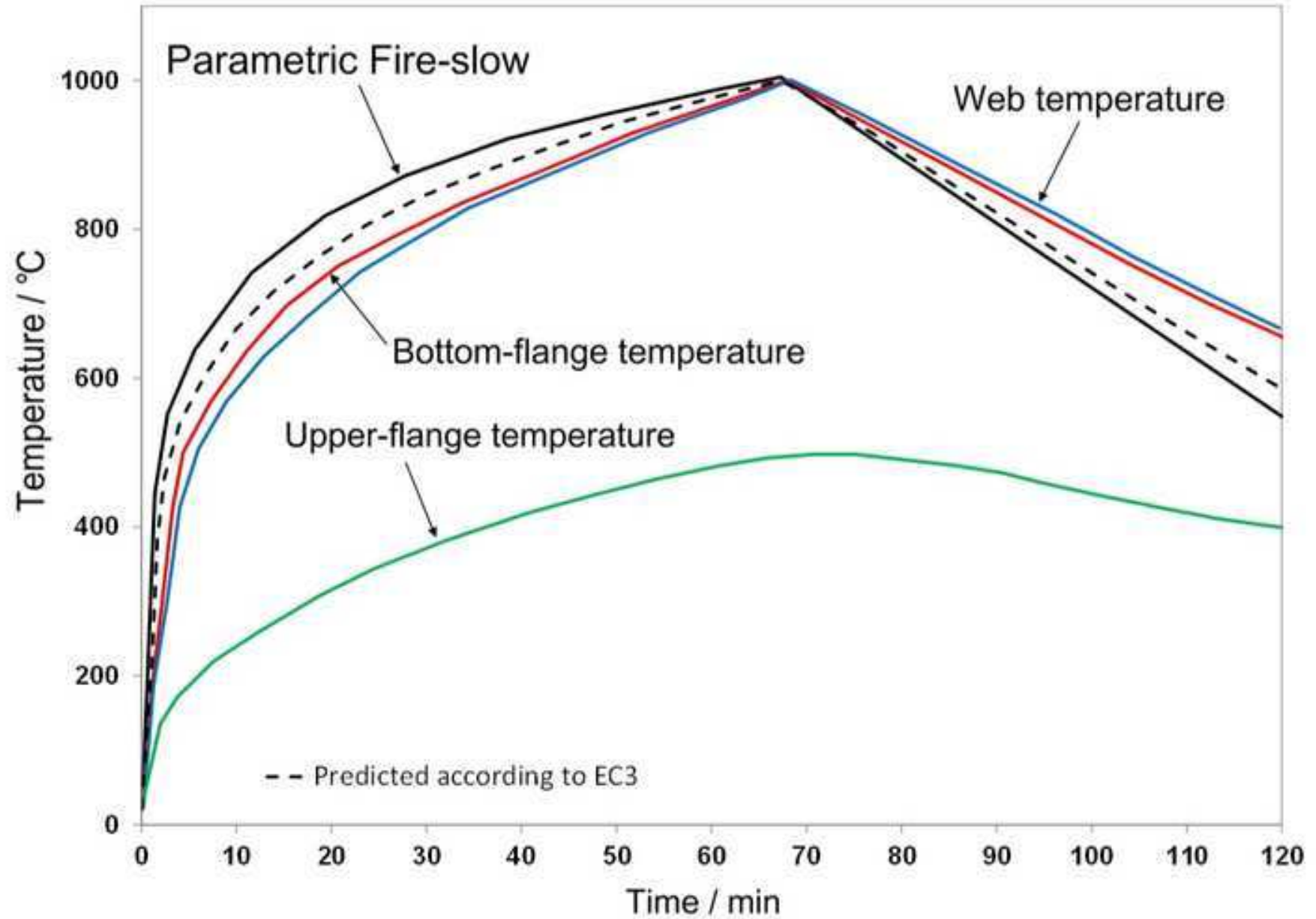


Figure 10d

[Click here to download high resolution image](#)

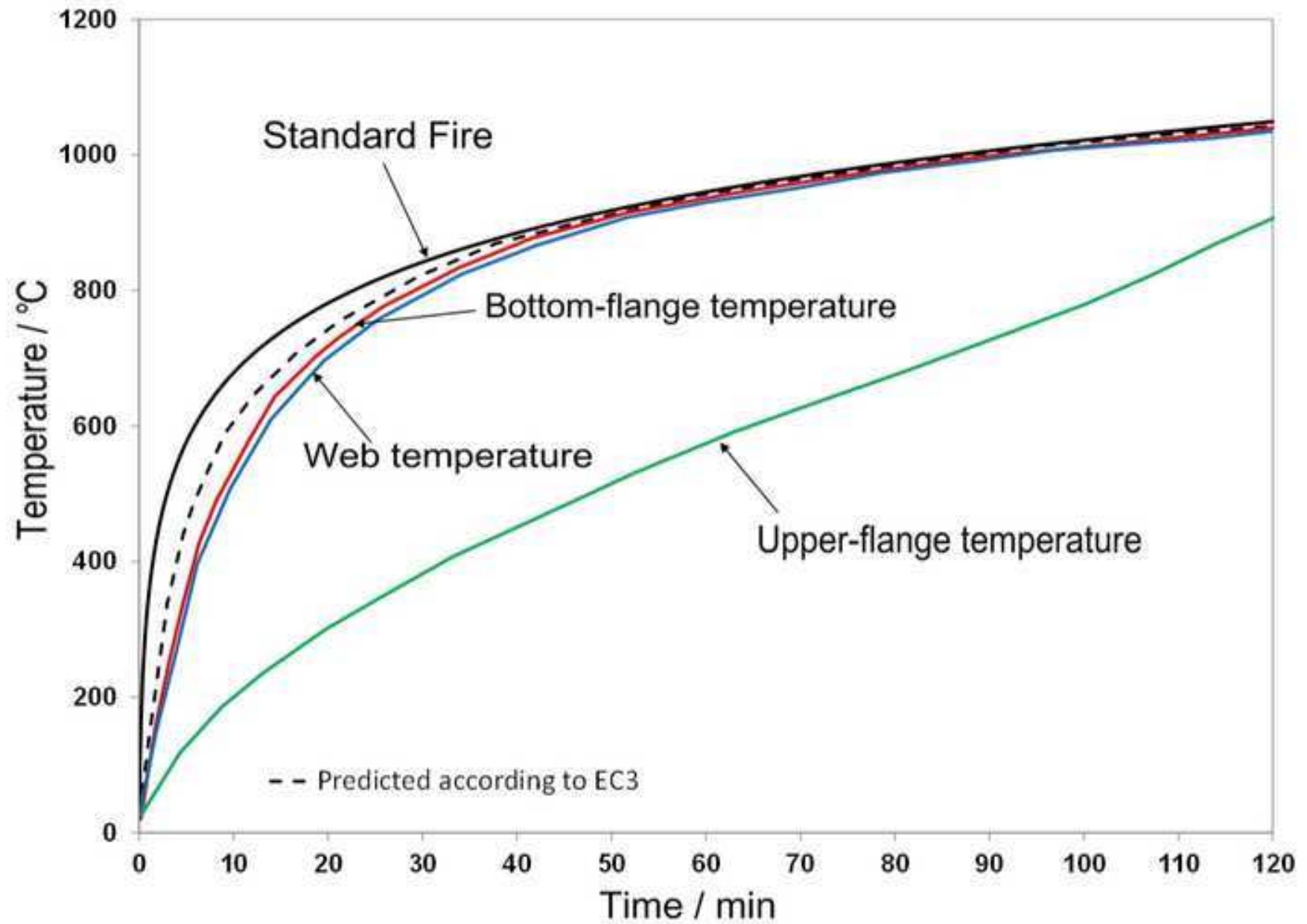


Figure 11

[Click here to download high resolution image](#)

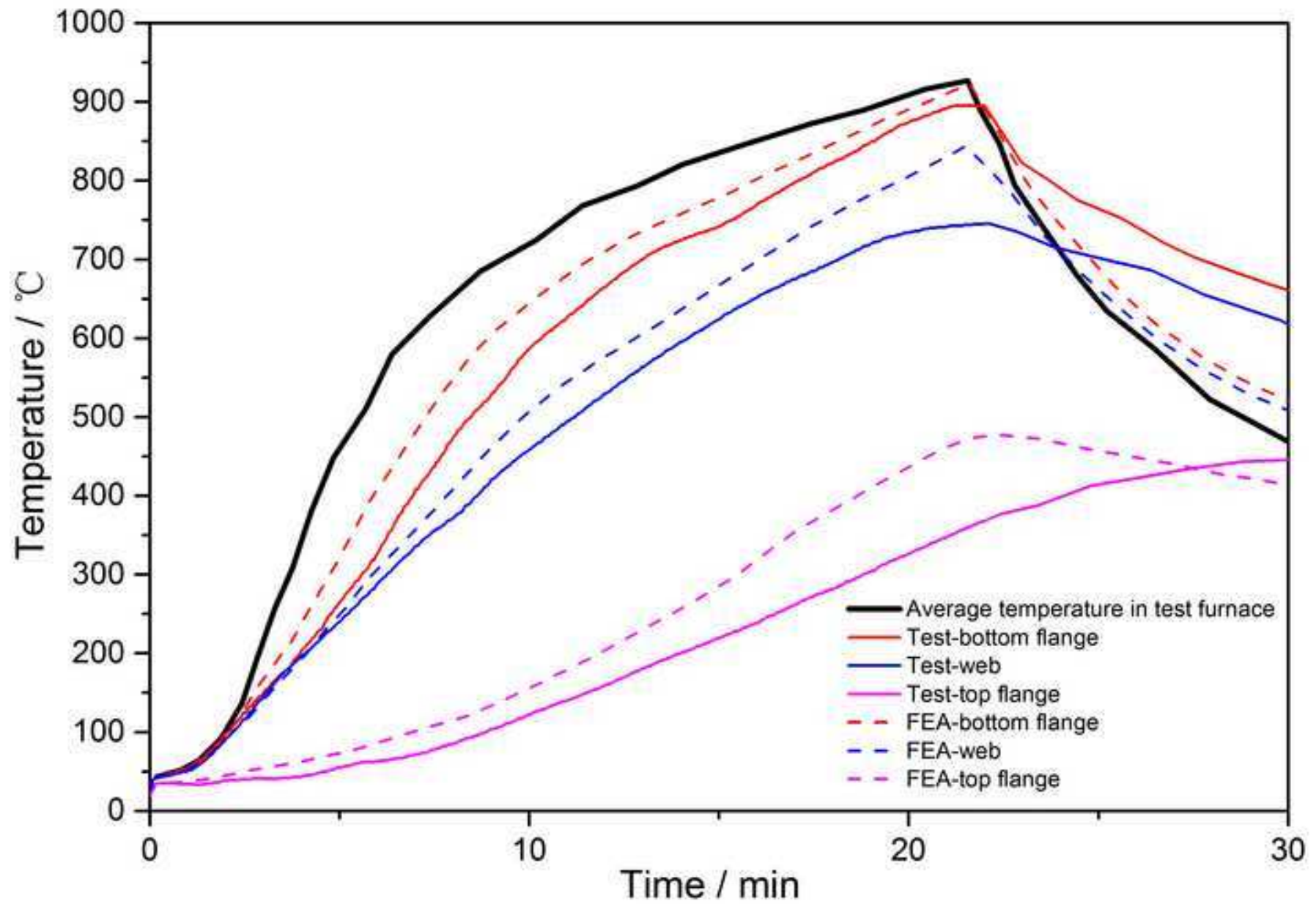


Figure 12

[Click here to download high resolution image](#)

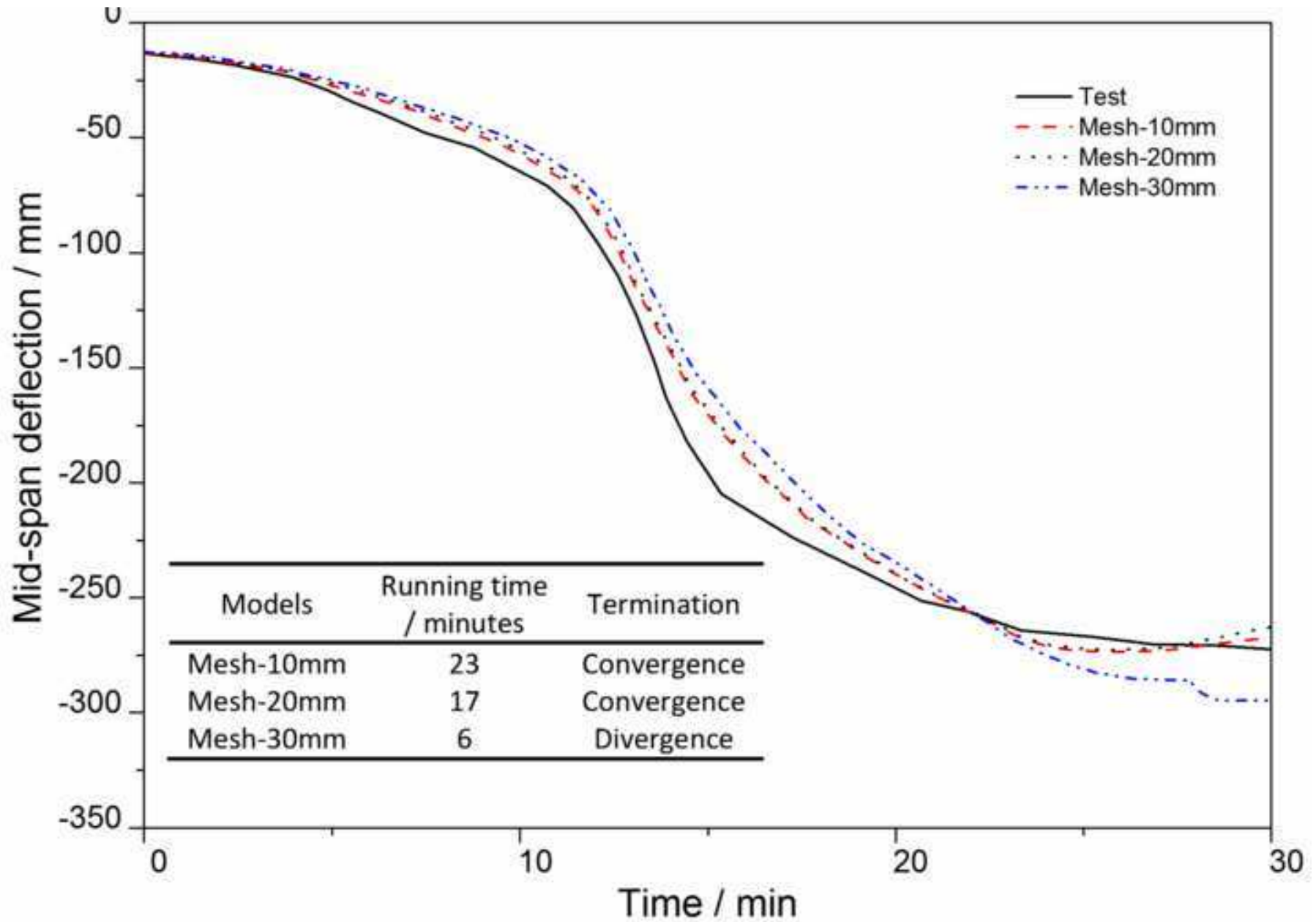


Figure 13a

[Click here to download high resolution image](#)

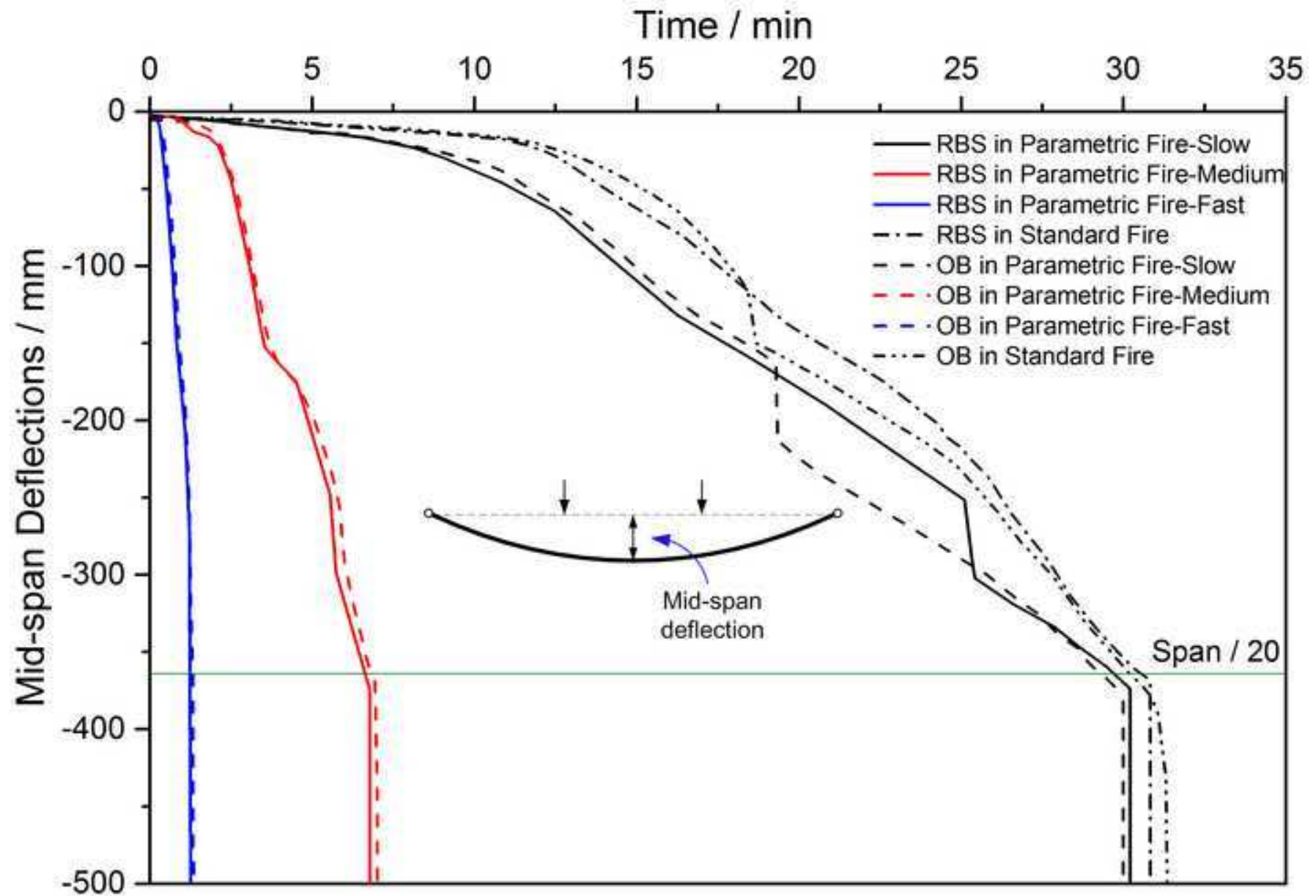




Figure 13b

[Click here to download high resolution image](#)

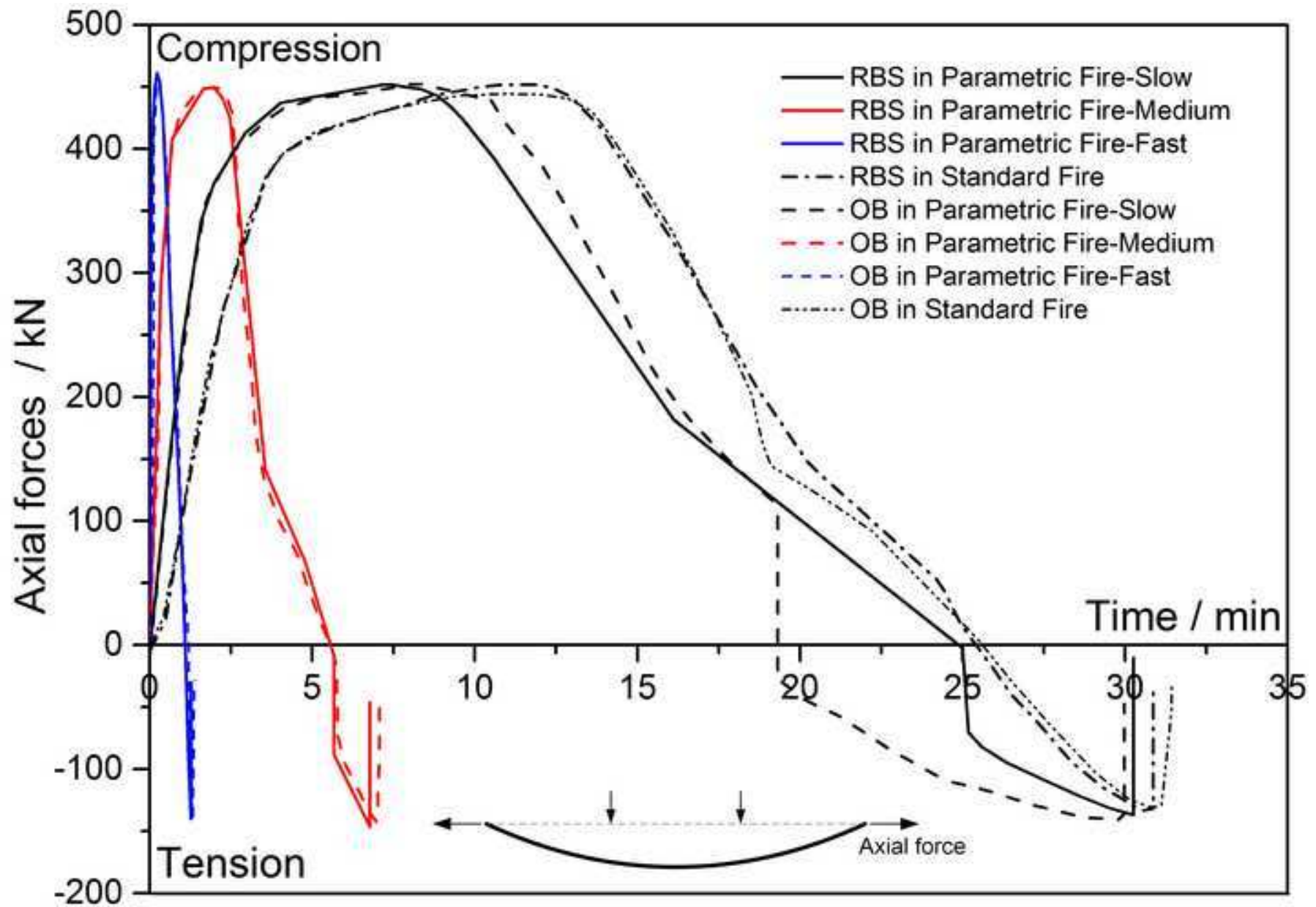


Figure 14a

[Click here to download high resolution image](#)

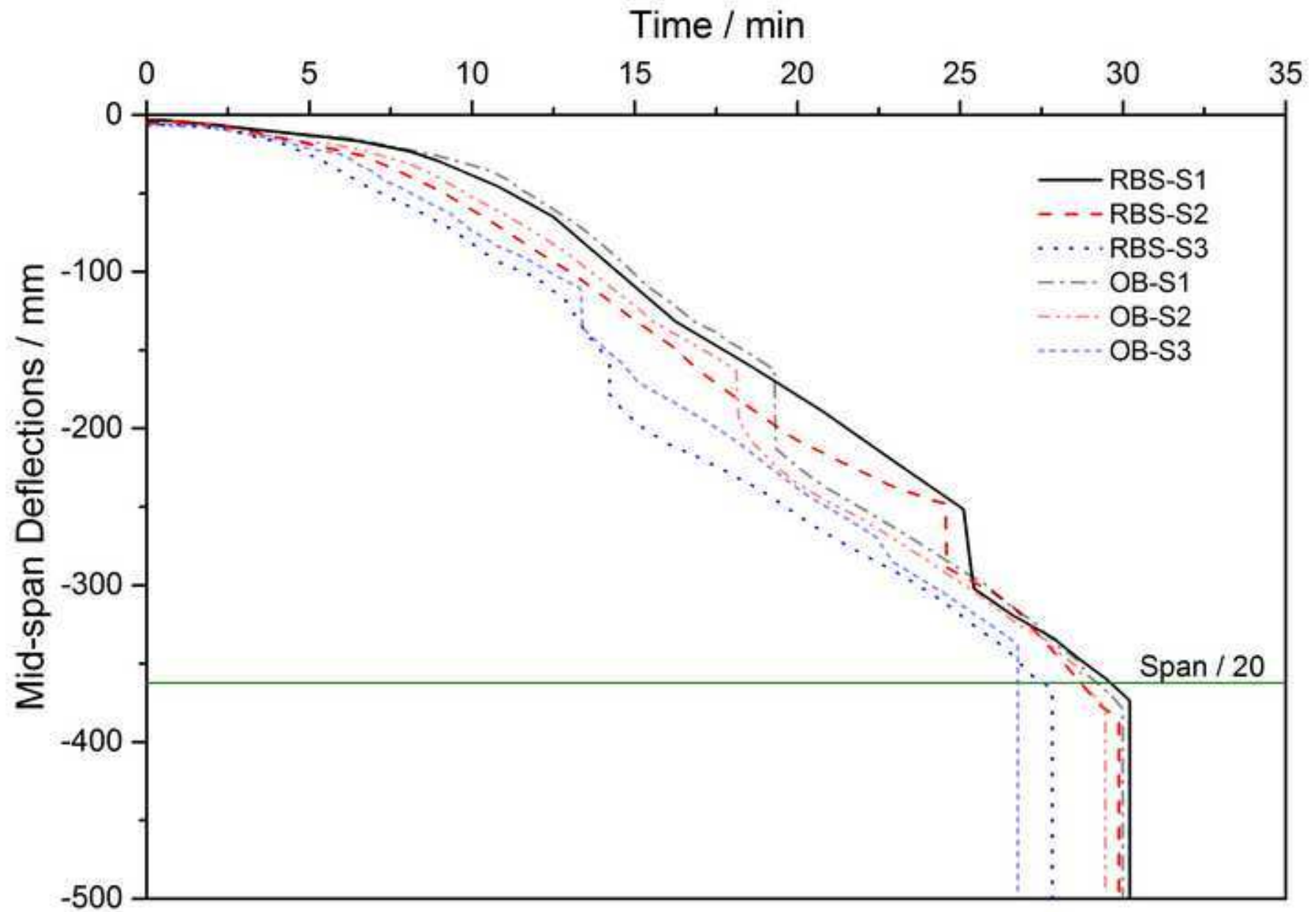


Figure 14b

[Click here to download high resolution image](#)

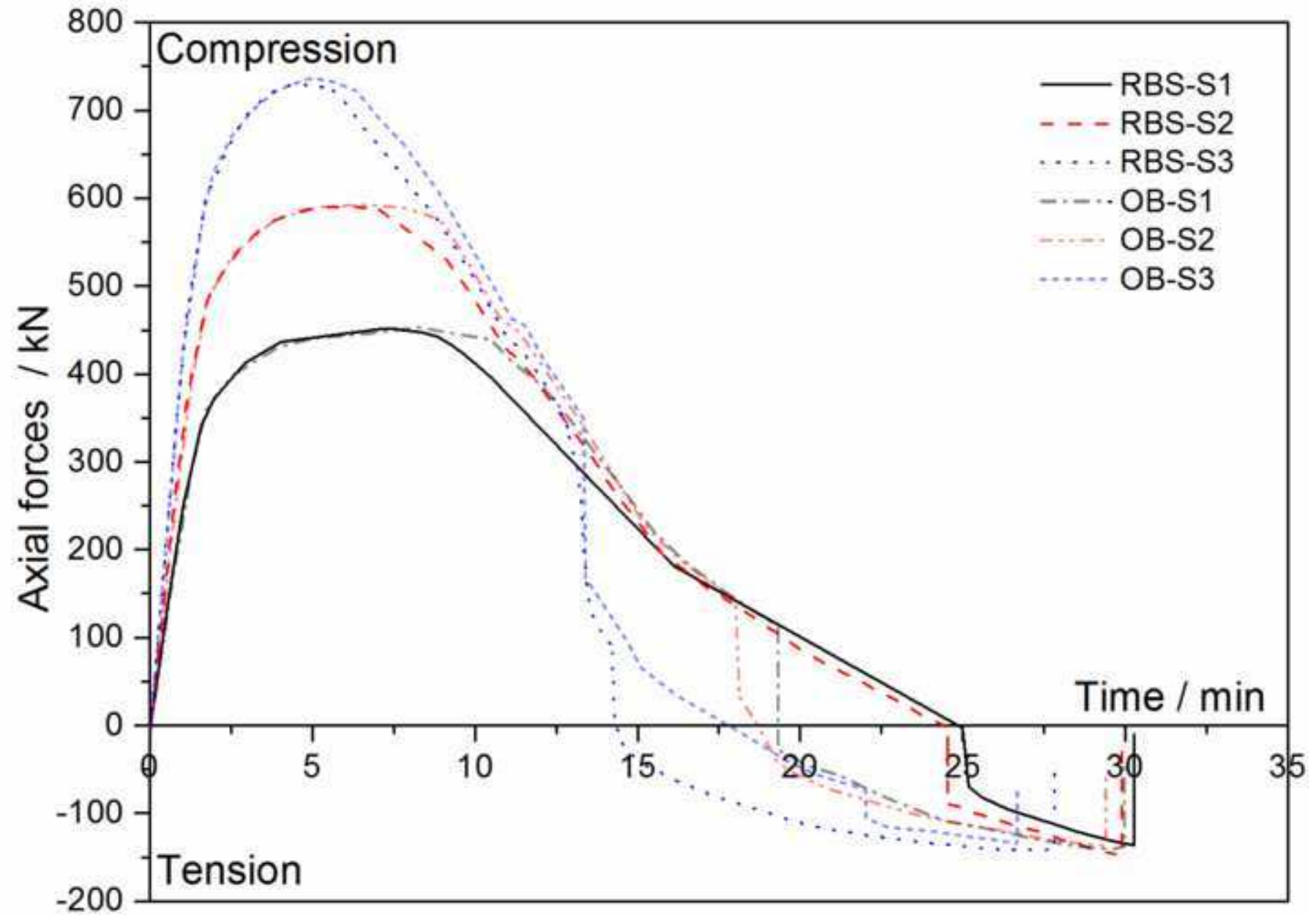


Figure 15a

[Click here to download high resolution image](#)

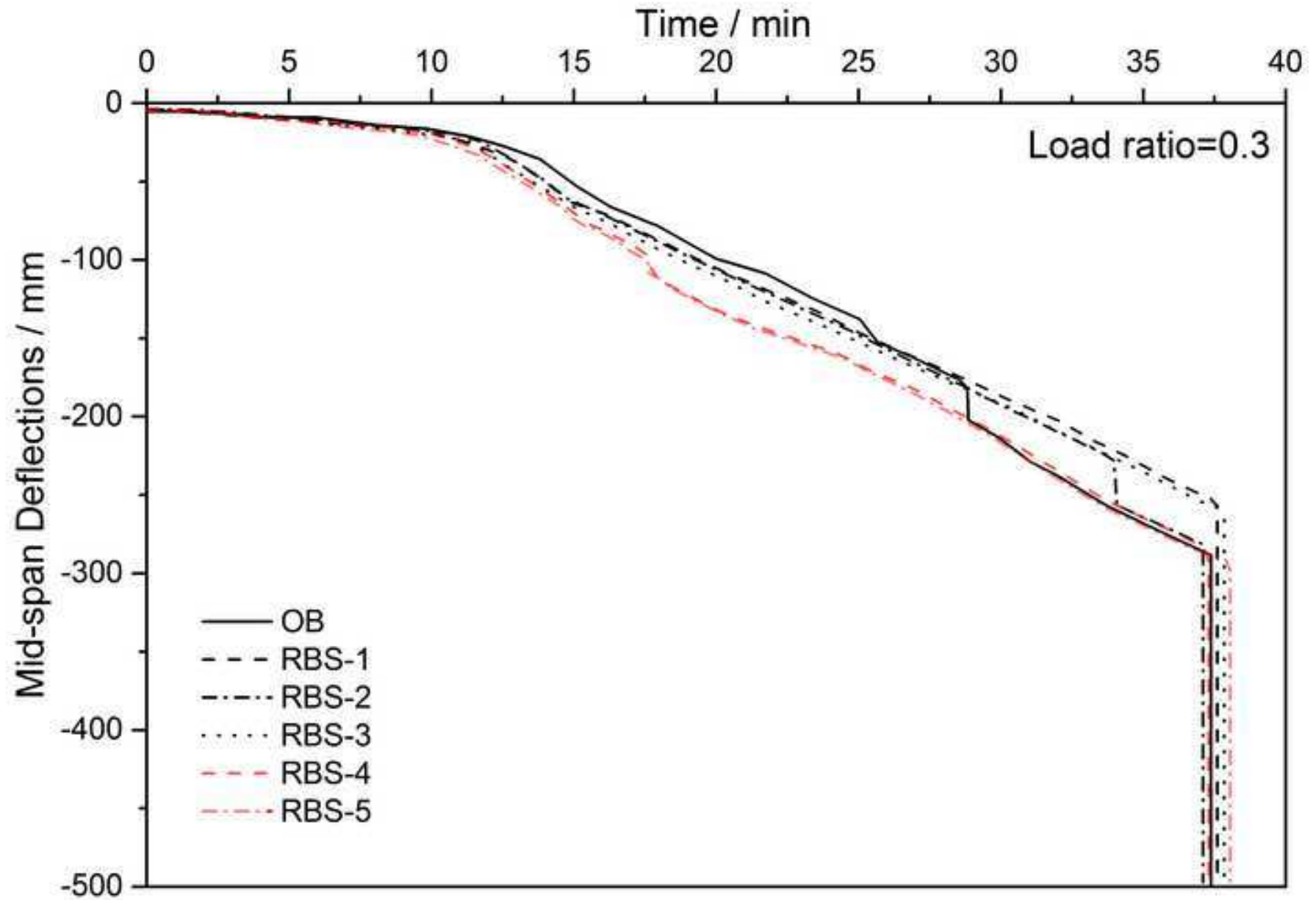


Figure 15b

[Click here to download high resolution image](#)

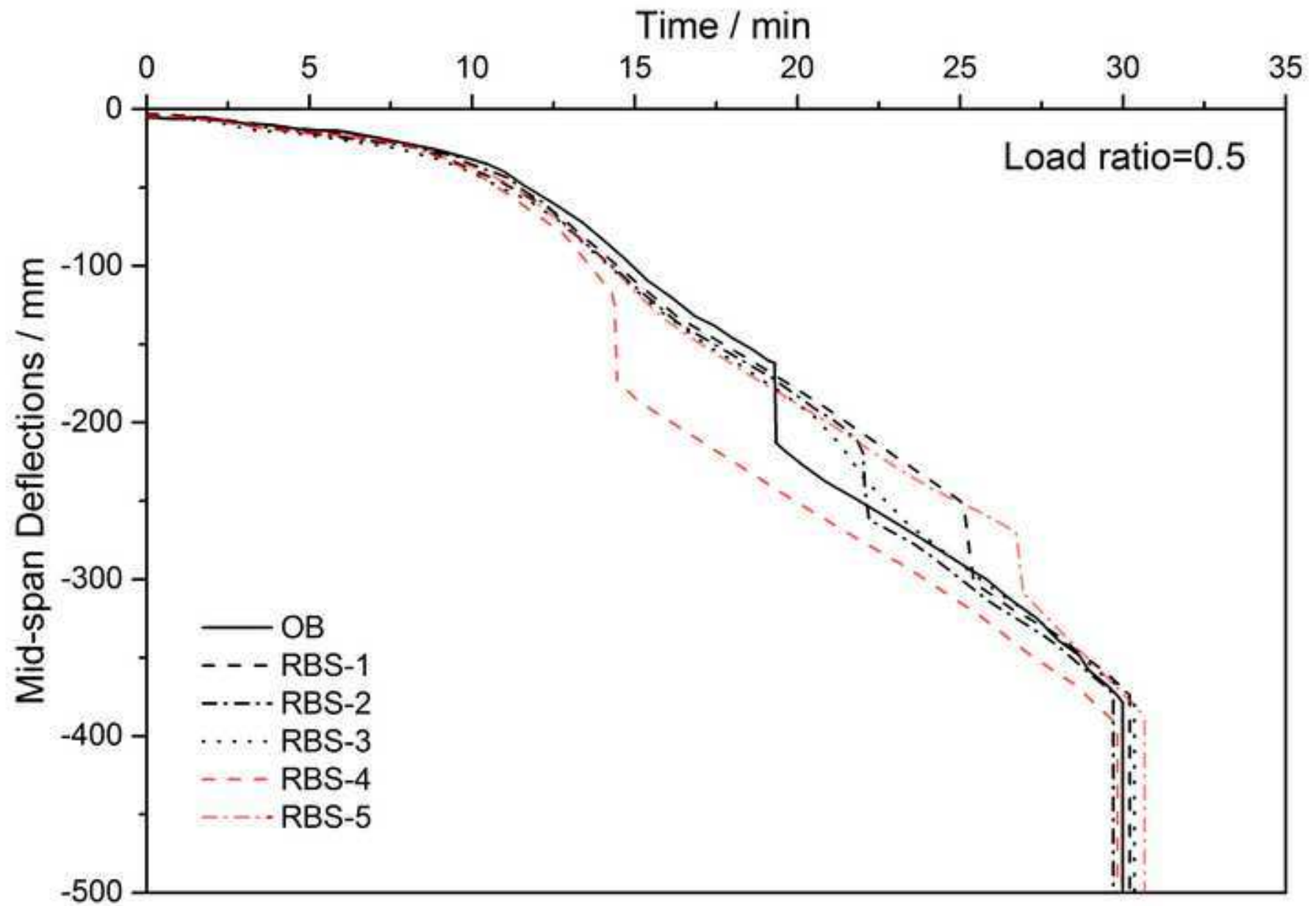


Figure 15c

[Click here to download high resolution image](#)

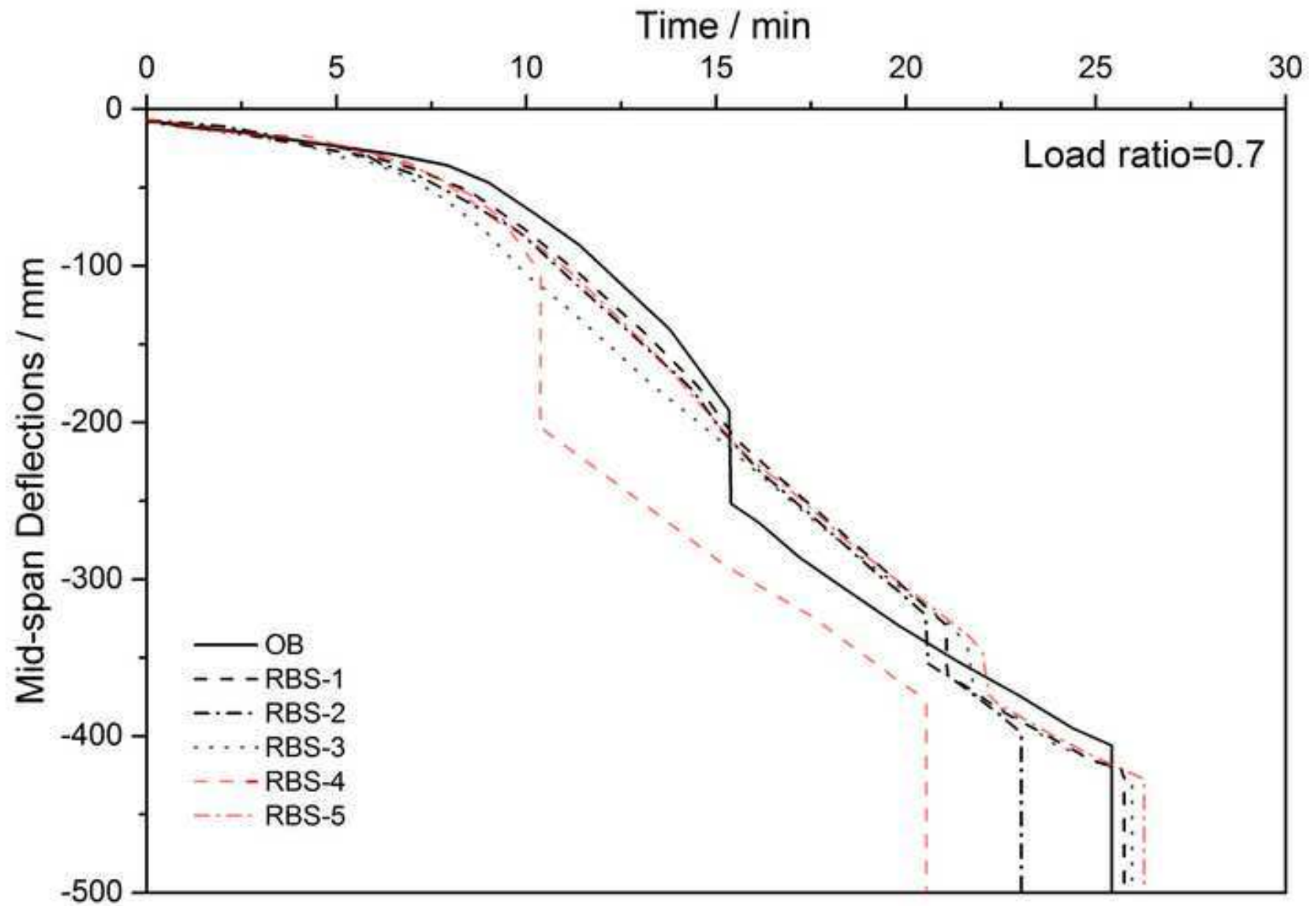


Figure 15d

[Click here to download high resolution image](#)

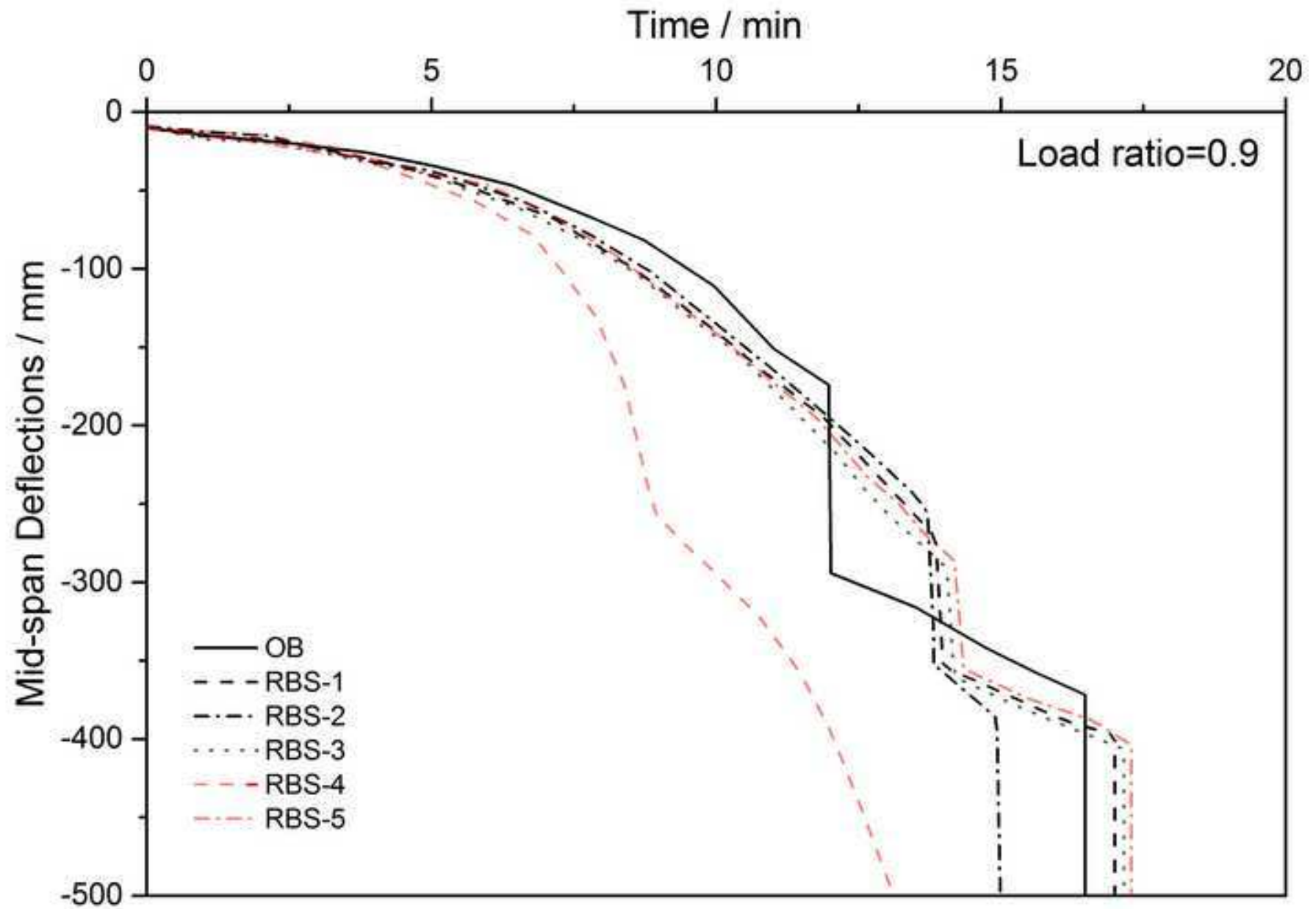


Figure 16a

[Click here to download high resolution image](#)

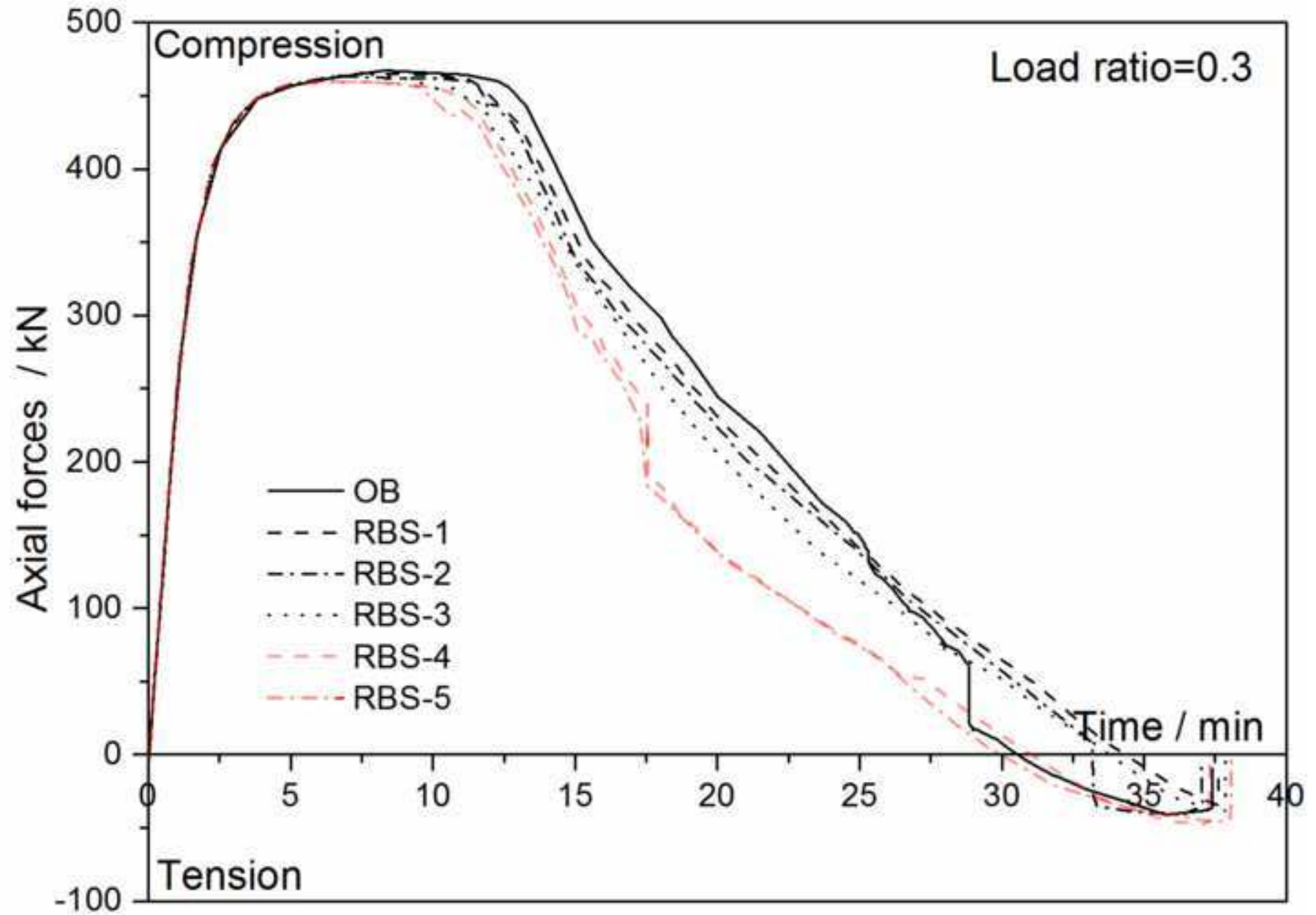




Figure 16b

[Click here to download high resolution image](#)

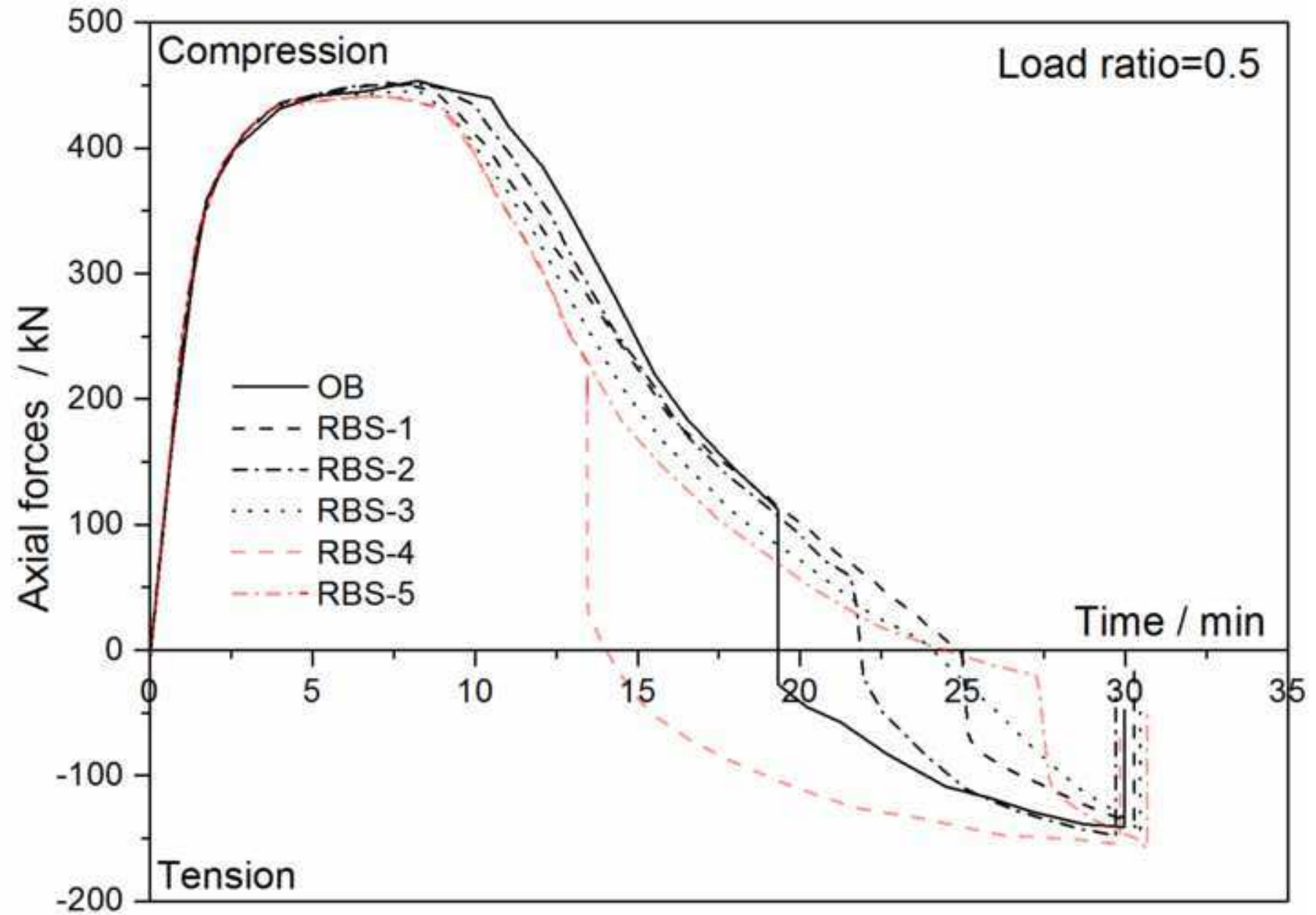


Figure 16c

[Click here to download high resolution image](#)

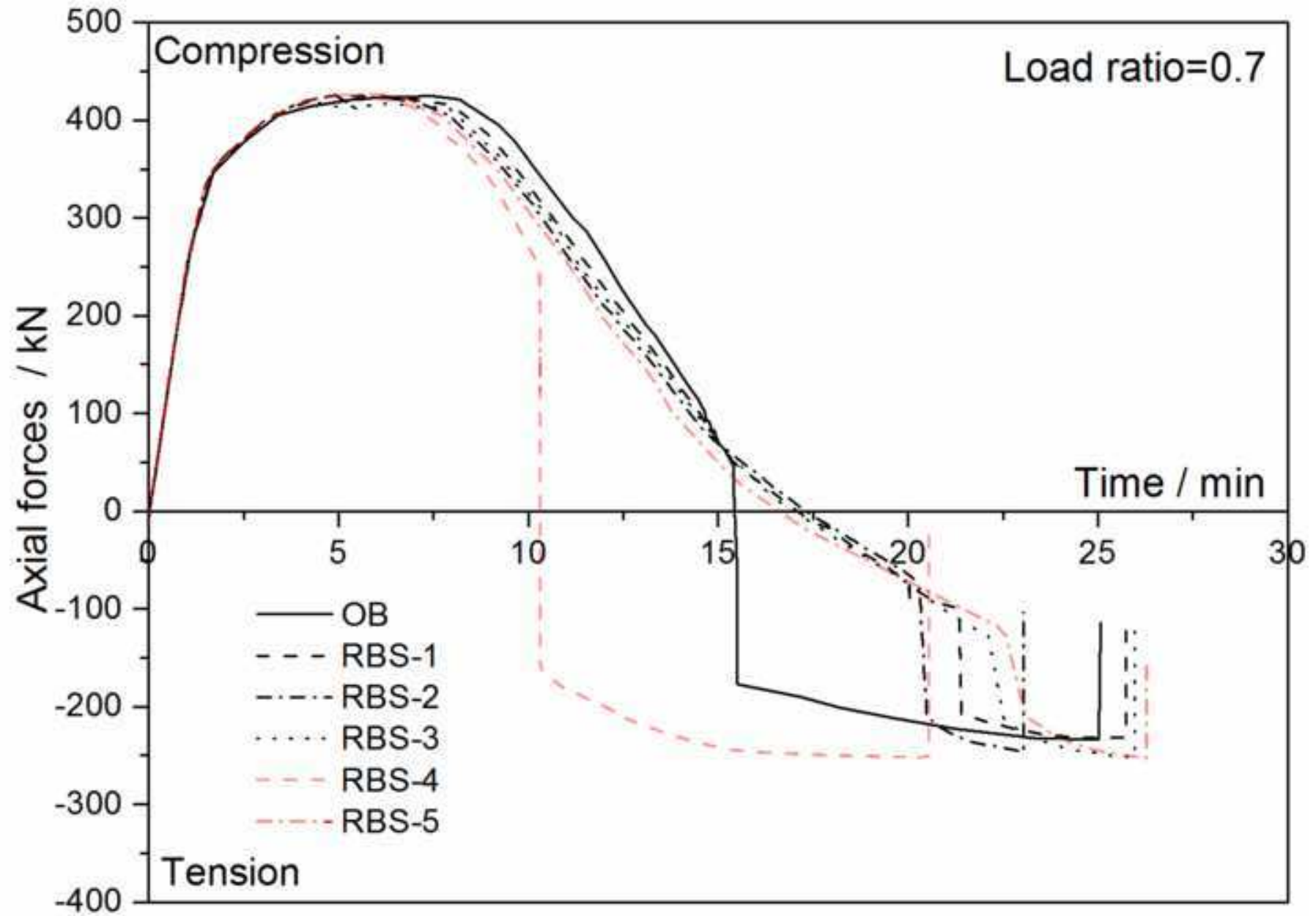


Figure 16d

[Click here to download high resolution image](#)

